The onshore and offshore groundwater salinity distribution between Egmond aan Zee and Castricum aan Zee

Author: P. S. Pauw
Supervisors: J. Groen (VU Amsterdam / Acacia Water), M.M.A. Groen (VU Amsterdam) and V.E.A. Post (VU Amsterdam)

Amsterdam, December 2009
Master Thesis Hydrogeology; O variant (27 ECTS)
Course code: 450122

vrije Universiteit amsterdam

Cover: Set up of a CVES measurement at the beach.

Index

1 Introduction

1.1 The Ecobeach pilot

Parts of the coast of the Western Netherlands are subjected to structural marine erosion. In 1990, the Dutch government defined the Basic Shoreline and decided to maintain its position. Consequently, an average amount of 12 million m^3 sediment has to be supplied every year at the beach and near the shore (Caljouw, 2000). These nourishments lead to high public costs which are thought to increase in the future because of sea level rise (Oude Essink, 1996). In addition, they have a negative impact on the ecology of the shore and adjacent dune area (Janssen, 2008).
In 2006, the Royal BAM Group and Dutch Department of Public Works started the pilot 'Ecobeach' at the beach in the area around Egmond aan Zee and Castricum aan Zee (Figure 1.1). Vertical drainage pipes were installed in rows perpendicular to the coast, in between the high and the low water line. For a detailed description of these so called Pressure Equalizing Modules (PEMs), reference is made to EcoShore International Inc. (EcoShore, 2006). More information about the Ecobeach pilot can be found online (Ecobeach, 2006; www.ecobeach.nl). A comparable pilot system has been installed in Denmark in 2005 (Jakobsen and Brøgger, 2007). These systems are thought to stimulate beach accretion. However, reasonable proven explanations have not been provided yet. One of many hypotheses is that PEMs function as drains and thereby lower the water table at the beach. In general, beaches with relatively low groundwater tables tend to favor net sediment transport to the shore, while beaches with higher groundwater tables are usually associated with erosion (Horn, 2006).
In order to obtain a physical explanation for the influence of the PEMs on beach sediment transport, research has been carried out by J.J. Pieterse (Pieterse, 2009). His research was funded by the Royal BAM Group and the Innovation Program of the Dutch Department of Public Works (WINN). Several measurement results presented here were of use in the study performed by J.J. Pieterse, and are therefore funded by the Royal BAM Group and WINN. Sediment transport is not concerned in this thesis. The general interest is the onshore and offshore groundwater salinity distribution along a shore-perpendicular transect crossing the southern Ecobeach pilot plot at the beach (see Figure 1.1 and 'Outline and general methodology).

1.2 Related previous research

Groundwater in the coastal dune area of the Western Netherlands has been studied intensively, e.g., Stuyfzand (1993), Bakker (1981). In view of groundwater flow systems*, the accent has often been on groundwater in the onshore subsurface, while considerably fewer studies have focused on groundwater flow near and toward the sea. In recent years however, the interest in the offshore continuation of groundwater flow systems has increased. Some studies have focused on submarine groundwater discharge from unconfined aquifers (e.g. Robinson et al. (2007b), Lebbe and Vandenbohede (2001), Prieto and Destouni (2005)). Others studied

* A groundwater flow system is defined as a coherent, three-dimensional unit of groundwater flow with one recharge and one or more discharge areas (Stuyfzand, 1993).

offshore fresh groundwater on a larger scale, with the emphasis on the presence and formation of submarine fresh groundwater tongues (e.g., Groen and Kooi (2001), Manheim et al. (2004)).

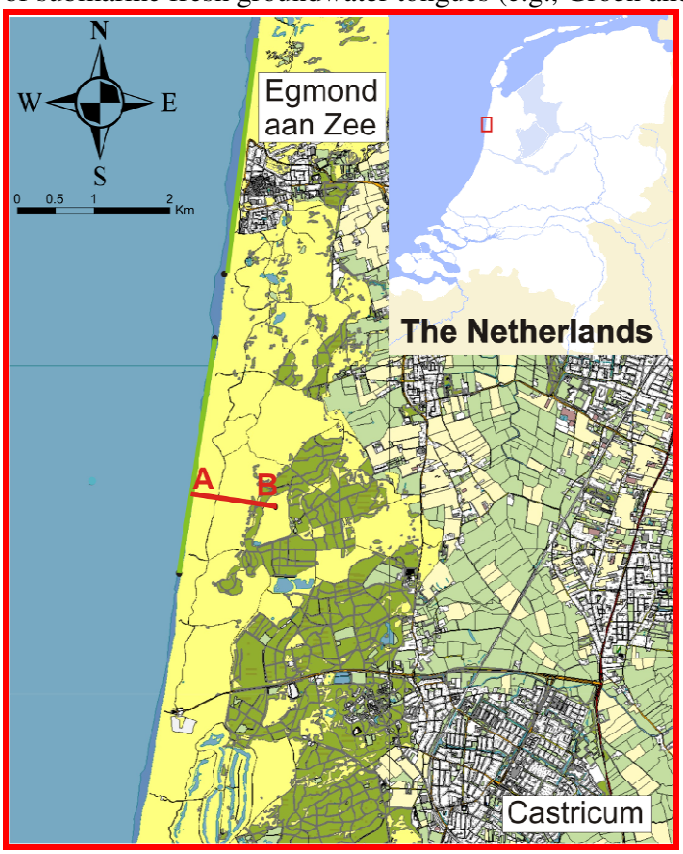

Figure 1.1 *Location sketch of the research transect (A-B, in red) and the Ecobeach pilot (in green). The pilot consists of two 3km long plots where PEMs have been installed.*

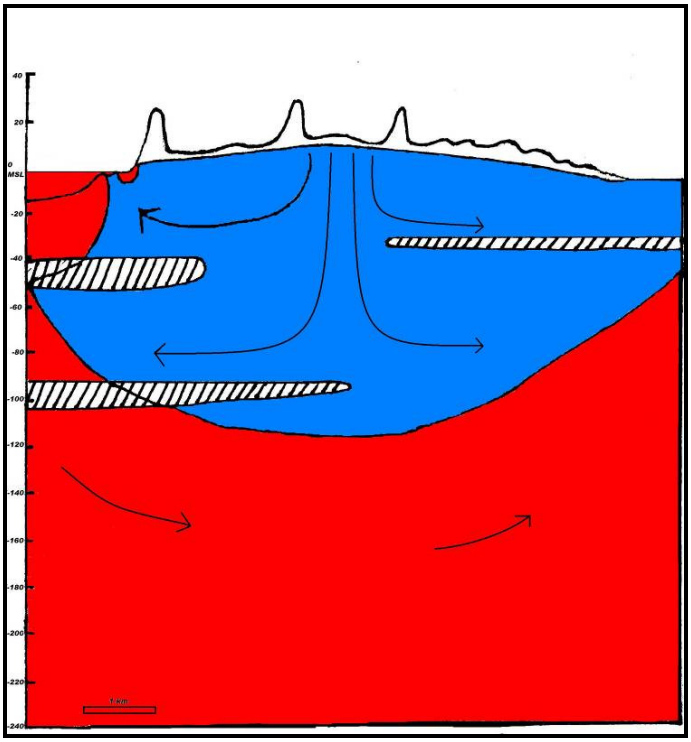

Figure 1.2 *Simplified schematization of the groundwater salinity distribution in the coastal dune area of the Western Netherlands. Low permeable units are indicated by uncolored regions with dashed lines. Salt water is indicated in red, fresh water in blue.*

A conceptual situation of the groundwater salinity distribution in the dune area of the Western Netherlands is shown in Figure 1.2. The freshwater lens is fed by excess precipitation. When alongshore groundwater flow is ignored, the horizontal flow components induced by topography driven flow from the dune area are directed to the polder areas and the North Sea. When low permeable sediments are present and continue offshore, a submarine freshwater tongue is thought to develop. When low permeable sediments are absent, the development of a submarine freshwater tongue is not expected.
Figure 1.2 also shows another groundwater flow component, which discharges across the seabed to the sea. In various literature, this flow component is defined as submarine groundwater discharge. Both components are of interest and will be discussed throughout this report.

1.3 Objectives

This thesis aims so give insight into the onshore and offshore groundwater salinity distribution in between Egmond aan Zee and Castricum aan Zee. More specifically it aims at:

- Mapping and simulating the distribution of fresh and saline groundwater in a cross section perpendicular to the coast.
- Investigate to what extent the current hydrological boundary conditions can explain the observed onshore groundwater salinity distribution.
- Giving insight into the dynamics of groundwater level, salinity and temperature at the beach, over a spring-neap tidal cycle.

1.4 Outline and general methodology

The onshore and offshore groundwater salinity distribution is investigated along a single transect perpendicular to the coast (Figure 1.1) using various field measurements and numerical model experiments. The primary focus is on this transect, but some field measurements were conducted at some distance from it for alongshore investigations of the groundwater salinity. The vertical extent of the research transect is determined at 150m –Mean Sea Level (MSL).
Two beach posts, marked “4200”, are located at the research transect and are used as a reference point for field measurements. Chapter 3 deals with the conducted field measurements. Several geophysical methods were used to investigate fresh and salt groundwater distributions. Groundwater levels in the dunes were measured using shallow wells to delineate the groundwater table and to define the groundwater divide. Groundwater levels and specific electrical conductivity (EC, at 25 ^{o}C) were investigated at the beach during a spring – neap tidal cycle using CTD divers. Chapter 4 deals with a numerical study of the research transect, using the variable density groundwater flow model SEAWAT (Guo and Langevin, 2002). Chapter 5 gives an integral discussion of the previous chapters. The conclusions of this study can be found in chapter 6.

2 Site Description

2.1 Research location and physiography

The research transect is located in between Castricum aan Zee and Egmond aan Zee (Figure 1.1). The most eastern point (X=103525, Y=510675)* of the transect coincides with the groundwater divide in the dunes. The most western point is located approximately 50m west of the average low water line (X=102283, Y=510854). Two dune ridges are present along the transect (figure 2.1). The mean sea level is assumed to be the same as the Amsterdam Ordinance Level (NAP).

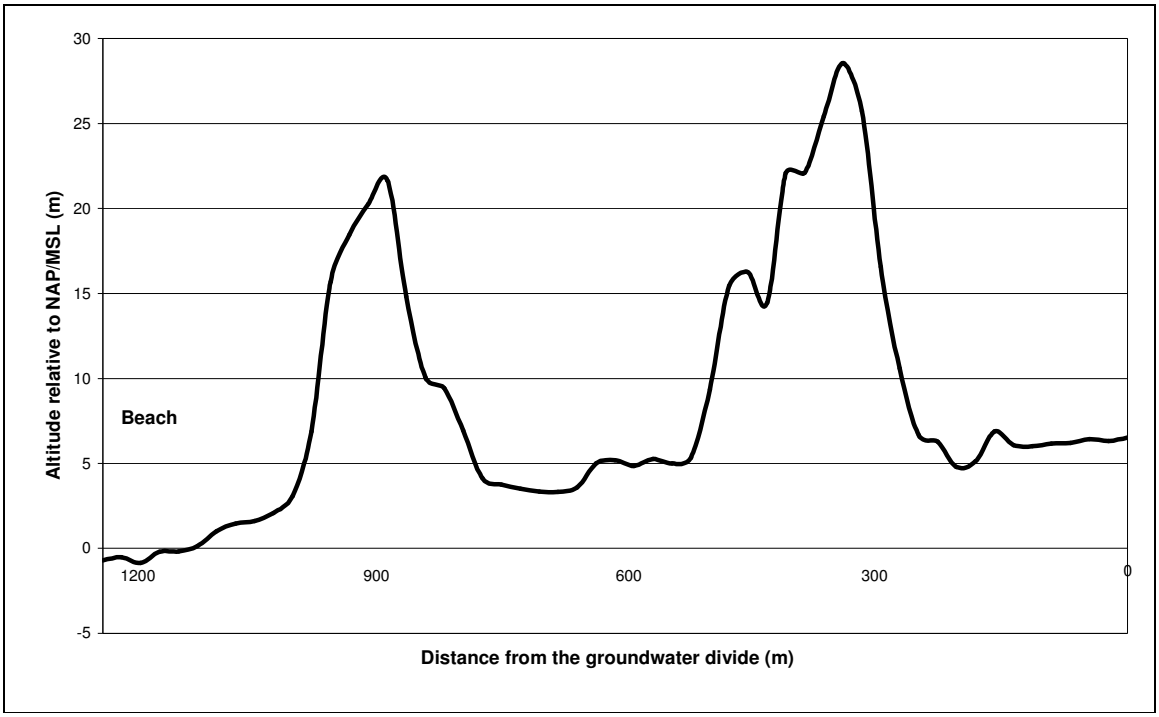

Figure 2.1 *Cross section showing the altitude variation along the 1250m research transect.*

2.2 Vegetation and climate

Vegetation at the beach is absent. The foredune ridge, the western side of the eastern dune ridge and the flanking valley are covered by marram, dune grasses, mosses, heather and sea buckthorns. A small patch of artificially planted pines and deciduous trees is present on the eastern side of the eastern ridge. These trees used to continue to the east, but have been removed recently (PWN, 2004). The climate of the region is maritime temperate (Köppen Cfb climate). Gross precipitation amounts 850mm on average. Maximum precipitation occurs in October and November (around 100mm on average), while minimum precipitation is in April and May (around 45mm on average) (KNMI, 2000).

* Coordinates according to the Rijksdriehoeksstelsel, the national grid system of the Netherlands.

2.3 Geology and soils

The geologic formations of the Quaternary that are of interest in this study reach to a depth of 360m -MSL. They consist of unconsolidated marine, eolian, fluvial and glacial sediments. Figure 2.2 depicts an overview. The information in this paragraph derives from Berendsen (2004).
The Maassluis formation consists of clay and fine to medium coarse sands, which were deposited in a shallow marine environment. The formation is present from approximately 250m to 360m –MSL. On top of the Maassluis formation, coarse sands of the Peize formation reach to a depth of 100m –MSL. These sediments were deposited by the presently extinct Eridanos river system. The Waalre formation located on top of the Peize formation consists of fine to coarse sands deposited by the river Rhine. At the research transect its thickness is only 5m. From 95m to 75m -MSL, medium fine to coarse sands of the Appelscha formation are present, which were again deposited by the Eridanos river system. The Urk and Sterksel formations consist of Rhine deposits and are both dominated by coarse sands. They are located between 50 and 75m –MSL. On the western side of the research transect, the top of the Urk formation is at 45m –MSL.
While the above described formations are more or less horizontally stratified within the research transect, the following younger formations are less horizontally stratified. Their distributions derive from hydrogeological profiles provided by PWN (Appendix A-D) and borehole data shown in Figure 2.3.
During the Saalian glacial, a large ice sheet covered large parts of the Netherlands. As a result, glacial till belonging to the Drenthe formation is present at the eastern side of the research transect, from 40 to 50m -MSL. After the Saalian, sealevel rose during the Eemian interglacial. Marine sediments of the Eem formation can be found on top of the Drenthe formation. In the western part of the research transect the Drenthe formation is absent. Here, the Eem formation is located on top of the Urk formation. The top of the Eem formation is around 32m –MSL. Fluvial sediments of the Krefteheye formation were deposited during the Eemian and Weichselian periods. They are absent on the eastern side of the research transect. In the middle of the transect they reach a thickness of 12m. The youngest formation present is the Naaldwijk formation, which consists of marine and eolian sediments. The lithology varies from clay to coarse sand, but medium fine sand is the dominant lithology here.
Around 1000 A.D., the formation of the present dune landscape began by the deposition of eolean sediments, belonging to the Schoorl member (Naaldwijk formation). From the second half of the 19th century, marram and pine forests were planted to reduce the sediment transport in the dune area. The relatively young substrate, sparse vegetation and low nutrient availability have resulted in a poor soil development. Where old, planted trees are present, soil development is slightly more pronounced.

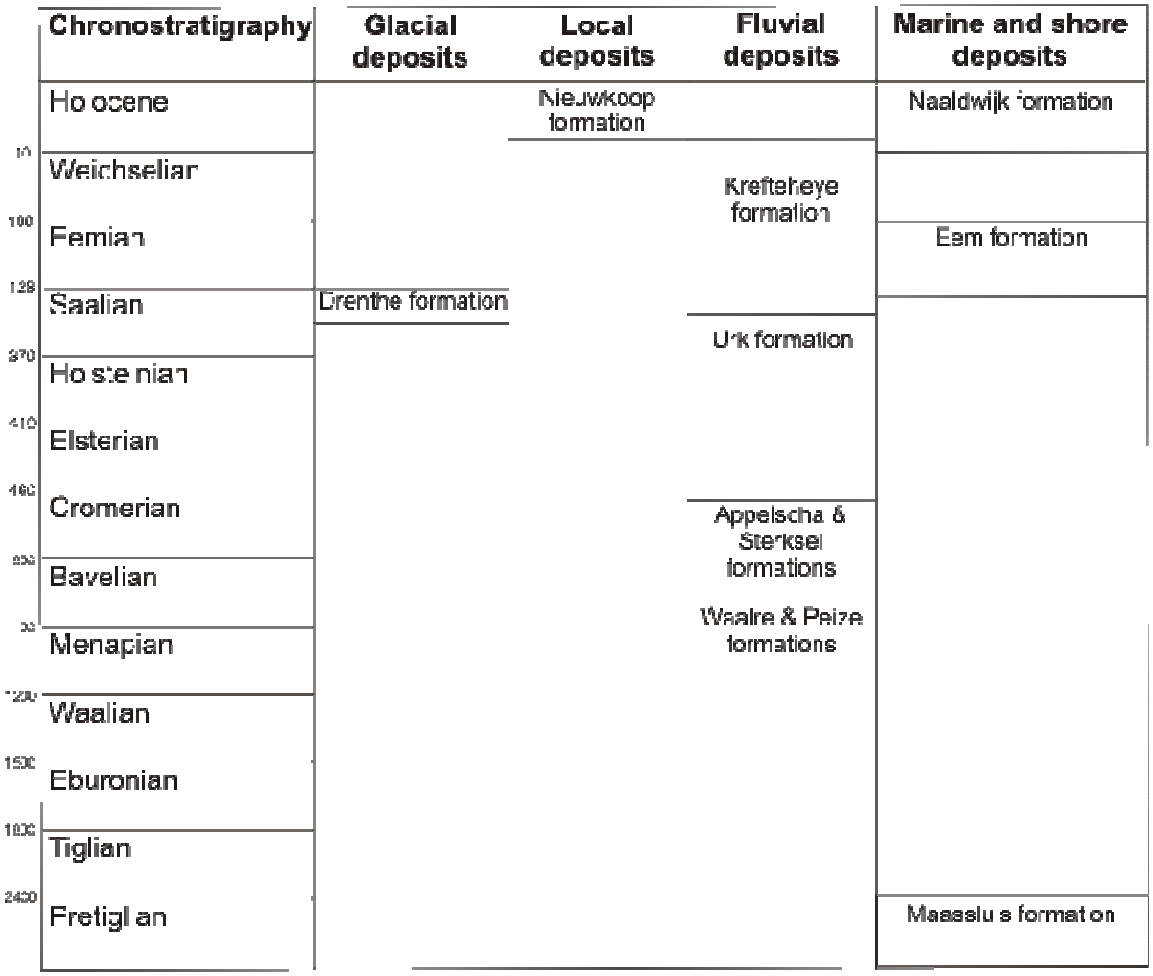

Figure 2.2 *Quaternary formations present at the research transect. The lithostratigraphy is based on the subdivision by Weerts et al. (2003). Numbers on the left side are time indications (in 10^3 yr). Modified after Berendsen (2004).*

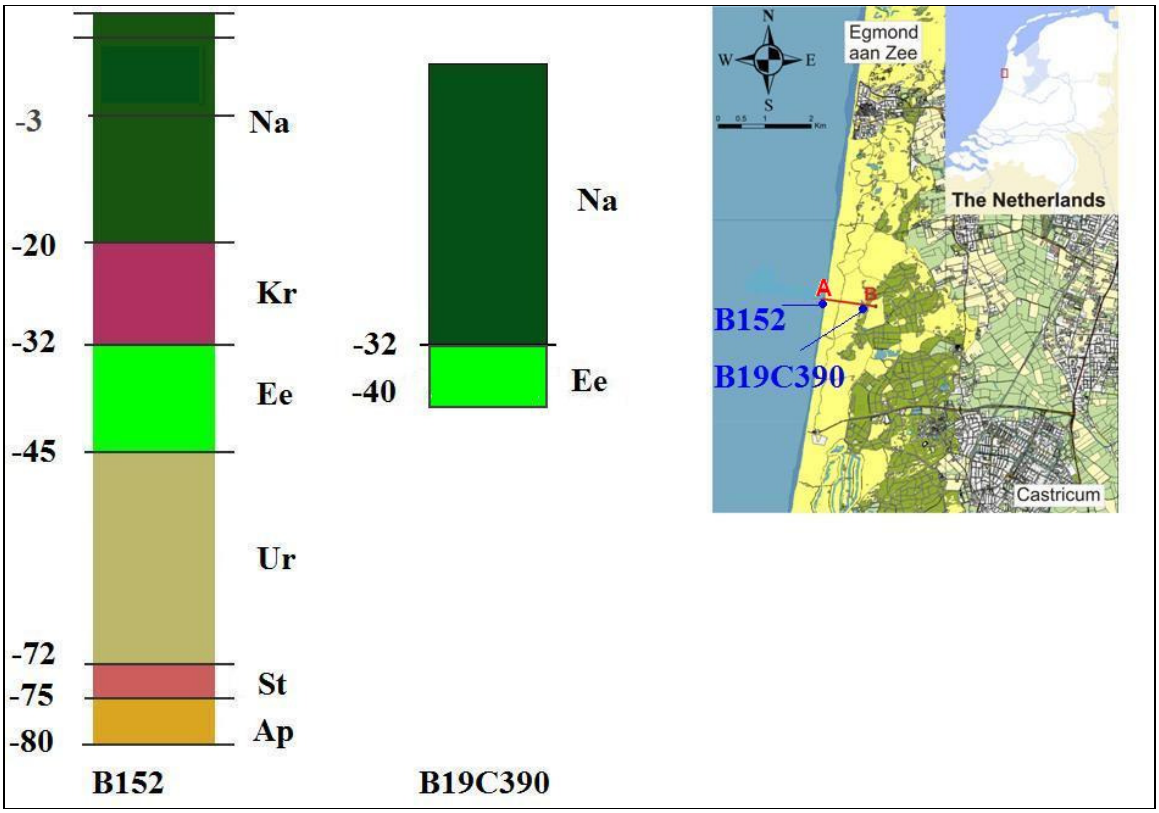

Figure 2.3 *Vertical distribution of several Pleistocene formations, derived from two borehole data sets (B152 and B19C390) available from Dinoloket (Dinoloket, 2009). The lithostratigraphic subdivision of borehole B152 has been made by Dinoloket, while B19C390 has been subdivided by the author. The different colours and codes correspond to the lithostratigraphic subdivision by Weerts et al. (2003) where: Na = Naaldwijk Formation, Kr = Krefteheye Formation, Ee = Eem Formation, Ur = Urk Formation, St = Sterksel Formation and Ap = Appelscha Formation. The location of the boreholes is indicated on the right. Numbers at the left side of the column indicate the depth relative to MSL.*

2.4 Hydrology

Recharge is assumed to be uniform along the research transect because vegetation differences are small and the transect is relatively short. Based on Stuyfzand (1993), annual recharge is between 300 and 400mm/yr.
Pumping activities take place just south of Castricum aan Zee, which is approximately 2.5km south of the research transect. Artificial recharge is applied here since 1957. From 1915 to 1961, water was pumped between 5 and 10m –MSL near Egmond aan Zee, but yielded small amounts of water compared to Castricum aan Zee. These pumping activities have been and are still influencing the interface of fresh and brackish/salt water and are most profound in the vicinity of the well fields. Near the research transect, the fresh-brackish interface rose less than 10m in the period 1910-1981 (Stuyfzand, 1993). Here it is assumed that the interface recovered after 1981.
The distribution of hydrogeological units near the research transect is shown in appendix B and C. From these hydrogeological profiles, a hydrostratigraphic subdivision was made for the numerical model experiments. This will be further discussed in chapter 4.

3 Field measurements

3.1 Introduction

Vertical Electrical Sounding (VES) and Continuous Vertical Electrical Sounding (CVES) measurements were performed at the beach to investigate the distribution of fresh and salt groundwater perpendicular to the coast. In order to examine alongshore variations, an electromagnetic survey was conducted using a frequency domain electromagnetic (FDEM) method. Time domain electromagnetic (TDEM) soundings were used to determine the deep fresh/salt groundwater interface at several locations in the dunes. All the geophysical measurements took place in the period November 2008 – February 2009.
Buried CTD divers were used to study groundwater levels, temperature and EC over time. These measurements were performed August and September 2009 (12 days). To identify the groundwater divide and delineate the phreatic level in the dunes, shallow wells were measured by hand. This was done in February and September 2009.
All methods are described in more detail in the following sections.

3.2 Methods

3.2.1 FDEM survey

A frequency domain method was applied using a Geonics EM-34 (McNeill, 1980) instrument. The EM-34 consists of two coils and two measurement devices which are connected by cables. The transmitting coil induces a primary electromagnetic field present above and below the ground. In the subsurface, conductive media induce eddy currents, which results in a secondary electromagnetic field. The secondary field differs in both phase and amplitude from the primary field, depending on the electrical properties of the subsurface. The receiving coil detects both primary and secondary fields. From this, the device will give a direct reading of the bulk conductivity of the subsurface. The instrument has three inter coil spacing's; 10m, 20m and 40m. In this study, the horizontal dipole configuration is used, where the coils are placed vertically on the ground. In this configuration the penetration depth is about $3/4^{th}$ of the inter coil spacing. In highly conductive ($\geq$ 100 milliSiemens/m (mS/m)) terrain, the EM-34 read out deviates from terrain conductivity (McNeill, 1980). Because these conditions prevail at the beach, the results are treated more qualitatively.
During a survey in November 2008, 6 transects perpendicular to the shoreline were investigated (Figure 3.1). Every 5 meter a measurement was taken with the 10, 20 and 40m coil spacing, starting from the dune foot and ending near the low water line. The coils were orientated parallel to the shoreline.

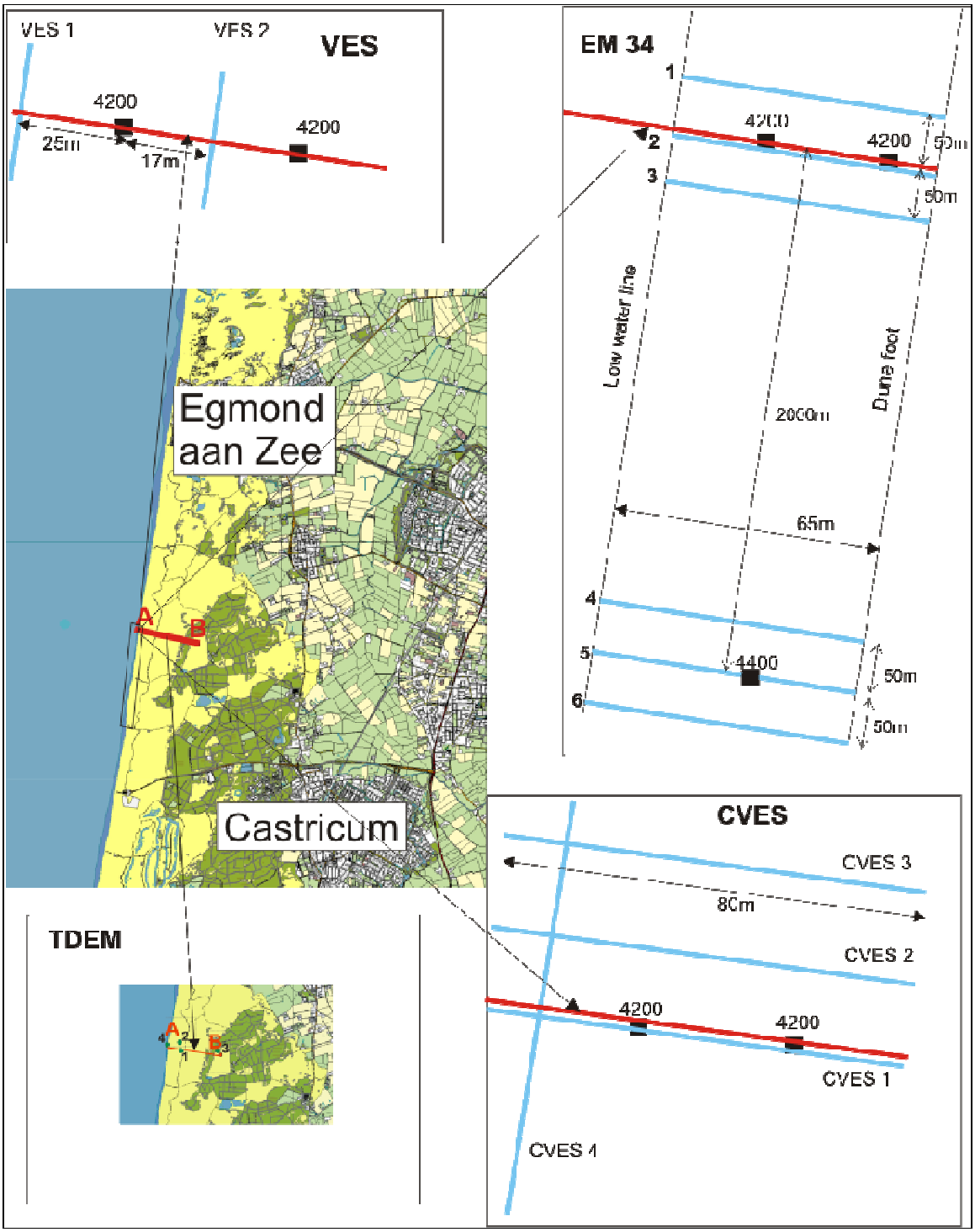

Figure 3.1 *Overview of all geophysical measurements. The beach posts are indicated by black squares. The research transect is indicated by a red line. The blue lines indicate the measurement profiles of the CVES, VES and FDEM(indicated by 'EM 34') measurements. The transect line of the FDEM measurements represents the midpoint between the two coils, which were orientated parallel to the shoreline. Note that the zoomed sketches are not scaled and that the position of the low water line varies because the measurements were taken at different times.*

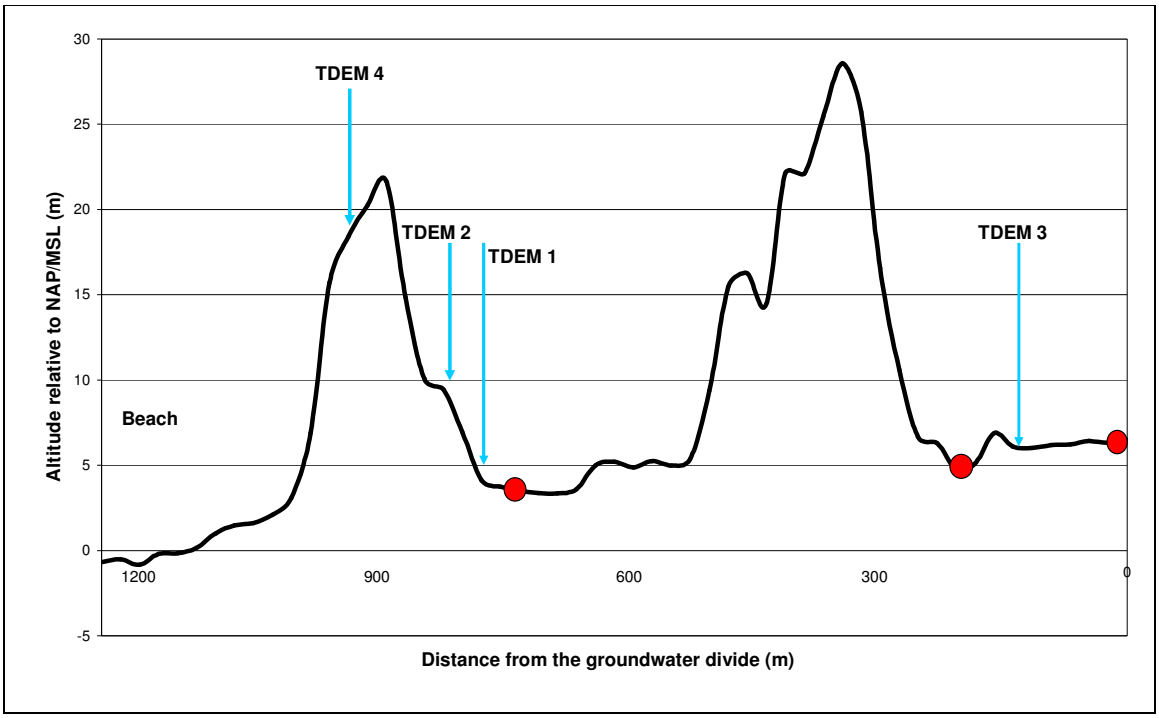

Figure 3.2 *Cross section along the research transect showing the locations of the TDEM (in blue) and water level (in red) measurements.*

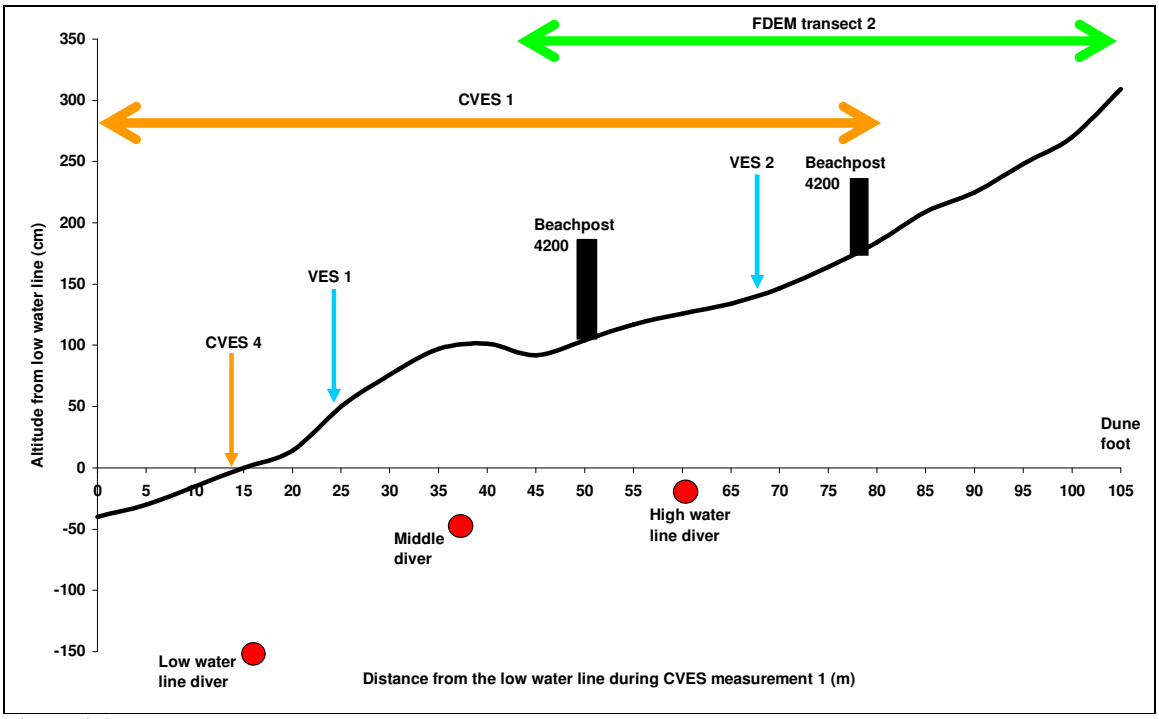

Figure 3.3 *Cross section along the beach area of the research transect showing all performed measurements there. The measurement numbers, e.g. CVES 4, coincide with the numbers shown in figure 3.1. The beachposts are indicated in black. The beach profile is based on level measurements at 26-08-2009, when the divers were installed.*

3.2.2 VES measurements

A VES is a method to determine the vertical variation in resistance of the subsurface. Two (current) electrodes placed in the ground are used to transmit a current (I; in Ampere) through the subsurface. Two other (potential) electrodes are placed in line and in between the current electrodes to measure the potential difference (ΔU; in Volt). The apparent resistivity (ρ_a; in Ohm) of the subsurface can then be calculated according to a modified form of Ohms Law:

$$\rho_a = G\frac{\Delta U}{I} \quad (3.1),$$

where G (in m) is a geometrical factor which depends on the configuration of the current and potential electrodes. For the VES measurements, a Schlumberger configuration was used. When the current electrode spacing is increased, the penetration depth increases so the measured apparent resistivity represents a larger part of the subsurface. The penetration depth depends on the resistivity of the subsurface. As a rule of thump, this depth is about one sixth of the distance of the current electrodes (van Breukelen et al., 2007).
From the apparent resistivity values obtained by the VES measurements, a model interpretation was carried out using the SCHLUMBG program (Hemker & Post, 2000). The resulting model consists of layers having different specific resistivity (ρ_s) values. From the specific resistivity values, fluid resistivity (ρ_f) can be calculated using a simplified form of Archie's law:

$$\rho_s = F\rho_f \quad (3.2),$$

where F is the dimensionless formation factor. The formation factor for sand is between 2 and 6. In clay, this relationship is not valid and should therefore not be used. Finally, fluid resistivity can be converted to EC (in μS cm^{-1}) using:

$$\rho_f = \frac{10000}{EC} \quad (3.3)$$

Two VES measurements were performed along the research transect using the ABEM Terrameter SAS 300 (ABEM, 1994). One (VES2) was located near the high water line, 17m east of the western beach post. The other one (VES1) was located near the low water line, 25 meter west of the western beach post (Figure 3.1 and 3.3). Both VES measurements were orientated parallel to the shoreline and had a maximum profile length of 600m.

3.2.3 CVES Measurements

A CVES can be seen as a joining up of multiple VES measurements, in order to obtain a two dimensional cross section image of the resistivity of the subsurface. The ABEM Lund Imaging System, enclosing the ABEM SAS 4000 terrameter and the ES10-64 electrode selector (ABEM, 2009), was used for the CVES measurements. CVES data were processed using the inversion program Res2Dinv (Geotomo, 1994). The Wenner configuration was applied for all CVES measurements instead of a Schlumberger configuration (applied with the VES), to reduce the measurement time. The measurement time was restricted to the low tide duration because all CVES measurements were taken in (a part of) the intertidal area of the beach. A maximum current of 1000mA, depending on the electrode distance and the subsurface resistance, was applied for all CVES measurements.
Four CVES measurements were performed in the end of January 2009 (Figure 3.1). CVES 4 was located near the low water line and was orientated parallel to the shoreline. The profile length was 400m, which resulted in a measurement depth of approximately 60m (Figure 3.14). The middle of the profile coincided with the research transect. Three CVES's were performed perpendicular to the shore, from the low water line to approximately 25m from the dune foot.

These had a profile length of 80m, which resulted in a measurement depth of 12m (Figures 3.11-3.13). CVES 1 was located at the research transect. CVES 2 and 3 were located respectively 50m and 100m north from here.

Figure 3.4 *Set up of a CVES perpendicular to the shore with a profile length of 80m. On the relatively dry part of the beach, the electrodes were placed deeper (0.5m) in the sand to cope with possible electrode contact problems.*

3.2.4 TDEM soundings

TDEM soundings were conducted in the dune area to determine the depth of the deep fresh-salt groundwater interface. The soundings are performed using an outer transmitter loop and an inner receiver loop, which were placed ungrounded at the surface. In the outer loop, a direct current is created which induces a primary electromagnetic field. When the current is turned off, a secondary electromagnetic field is created induced by eddy currents. The secondary electromagnetic field is decaying in time due to the resistance of the subsurface. The decay rate depends on the resistivity distribution of the subsurface.
The ZeroTEM (Zonge, 2000), enclosing the GDP 32-2 reciever and the NT20 transmitter, was used for the soundings. A 7A current was applied for all TDEM soundings, which was sufficient for a good signal/noise ratio. The loop configuration consisted of squares having 40m (outer loop) and 20m (inner loop) sides. Figures 3.1 and 3.2 show the locations of the TDEM soundings.

3.2.5 Water table measurements

Water table measurements on shallow wells and open water were performed in the end of January and the beginning of September to locate the groundwater divide and to verify the results (hydraulic heads) of the numerical experiments. Figure 3.2 shows the locations of these

measurements. It is assumed that the groundwater divide represents the border of water flowing in the direction of the ocean and water flowing towards the adjacent polder area.
The surface elevation was determined from the Actual Elevation Data for the Netherlands (AHN, 2009). The distance to the groundwater level was determined using measurement tape. Because the water table near the beach is significantly affected by the tides, the water table measurements in the valley were repeated in time to define an average hydraulic head.

3.2.6 CTD diver measurements

On August 26 2009, three CTD divers were buried in the beach sediment to monitor groundwater level, EC en temperature for a period of 12 days. The measurement interval was set to two minutes. The sensor of the diver was situated at 1.50m from the surface at the time of installation, to make sure that the divers remained under the groundwater table at all times. The diver was protected from the sediment by a polyethylene filter cloth. Beach morphology was monitored by using leveling equipment, were the most seaward located beach post functioned as a reference point. Groundwater levels were measured manually every day and used as an independent check of the diver measurements. The maximum wave run-up on the beach was observed for each tidal cycle by the author, to determine if the beach above the divers had been inundated during high water levels. By the time of installation, the distance from the low to the high water line was approximately 45m. One diver was installed at the low water line, and the other two were installed at 22.5m and 45m from here (Figure 3.3). Because data from a Barodiver was discontinuous and not complete, barometric compensation was performed using data from de Bilt (KNMI, 2009a), which is a meteorological station about 60km southeast of the research transect. Rainfall data was collected for the KNMI weather station at Wijk aan Zee, situated at approximately 10km south of the research transect (KNMI, 2009b).
The aims of these measurements were to deduce a boundary condition as an input for the numerical model (Chapter 4), and study the fresh and salt water dynamics of the beach groundwater over a period of 12 days, which approximately corresponded to a spring-neap tidal cycle period.

3.3 Results

3.3.1 FDEM survey

The results of the six transects per coil distance can be found in Appendix F. Little alongshore variation in apparent resistivity values was observed within transects 1-3 and 4-6. The mean apparent resistivity calculated for transect 1-3 (‘4200’) and 4-6 (‘4400’) for each coil distance are shown in figures 3.4 - 3.6. Because transects 4-6 are 5m longer than transects 1-3, an extra value has been added to the 4200 series at distance 0m which is the same as the 5m distance. For transect 2, which was measured on the research transect, the results of the three coil distances are plotted (Figure 3.8).

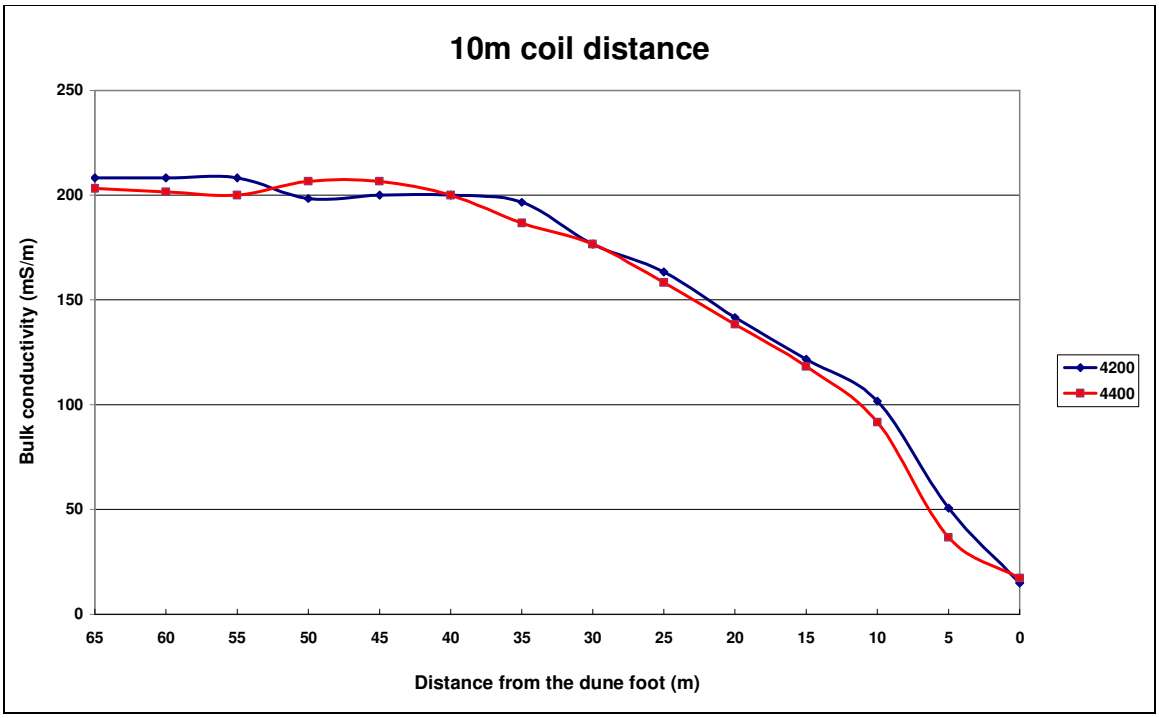

Figure 3.5 *Mean bulk conductivity of 3 transects near beach post 4200 (transect 1-3) and 4400 (transects 4-6), for the 10m coil distance.*

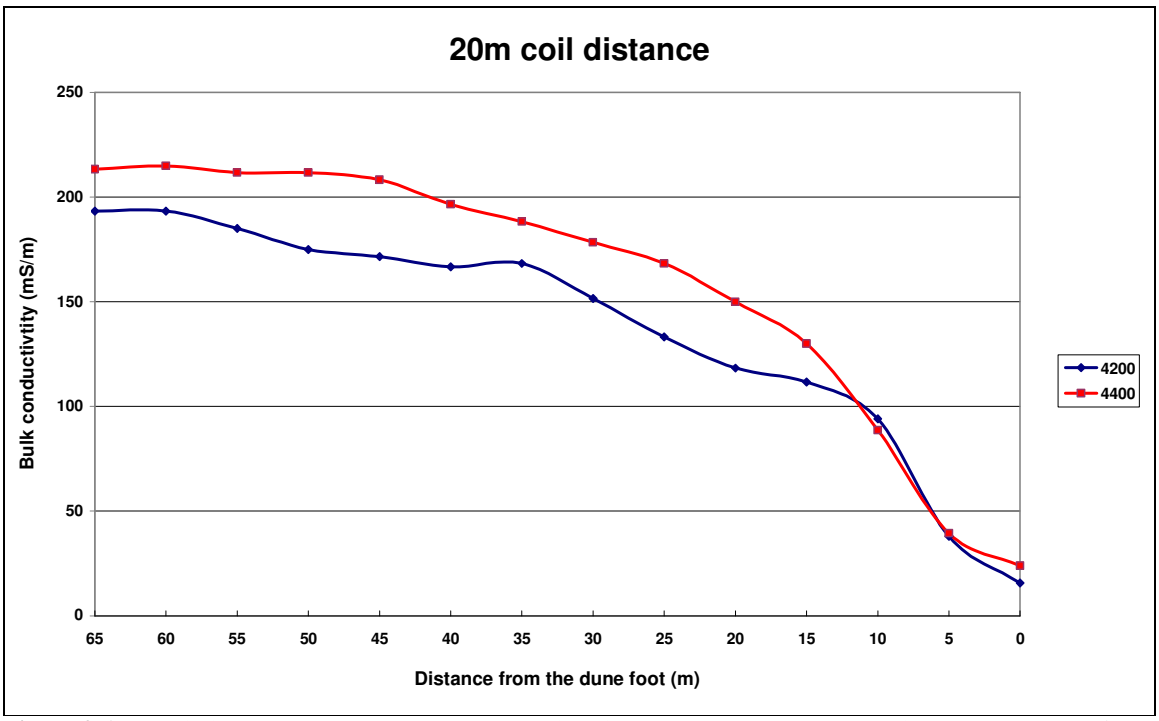

Figure 3.6 *Mean bulk conductivity of 3 transects near beach post 4200 (transect 1-3) and 4400 (transects 4-6), for the 20m coil distance.*

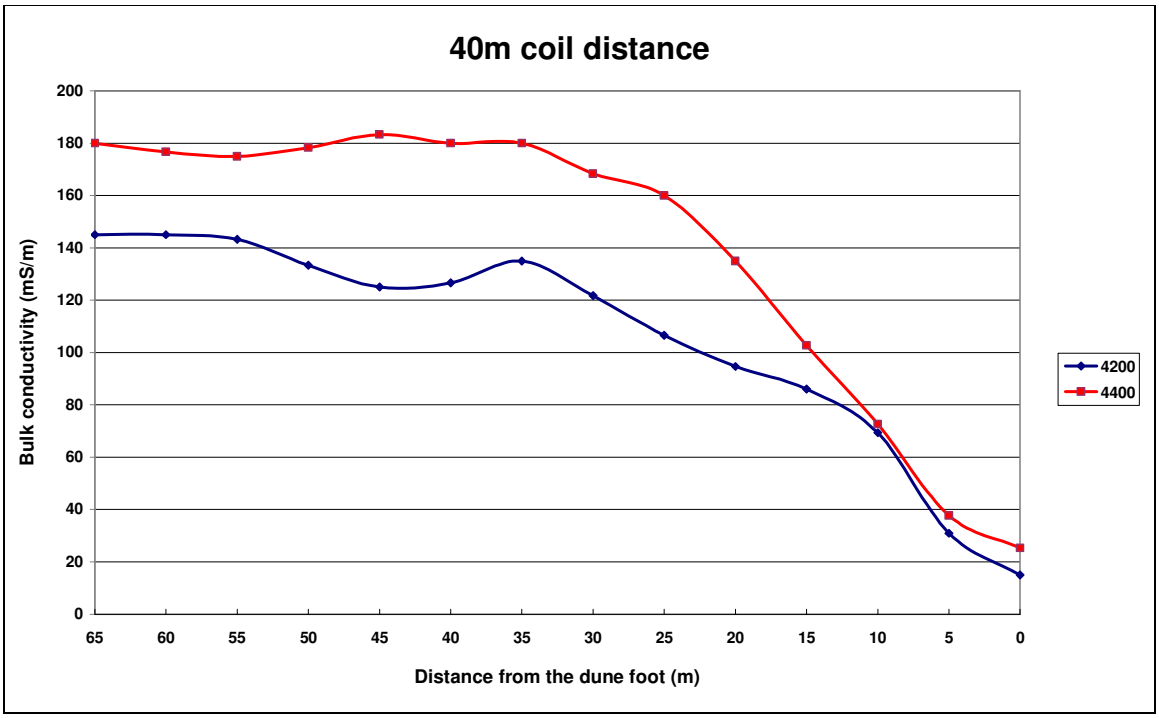

Figure 3.7 *Mean bulk conductivity of 3 transects near beach post 4200 (transect 1-3) and 4400 (transects 4-6), for the 40m coil distance..*

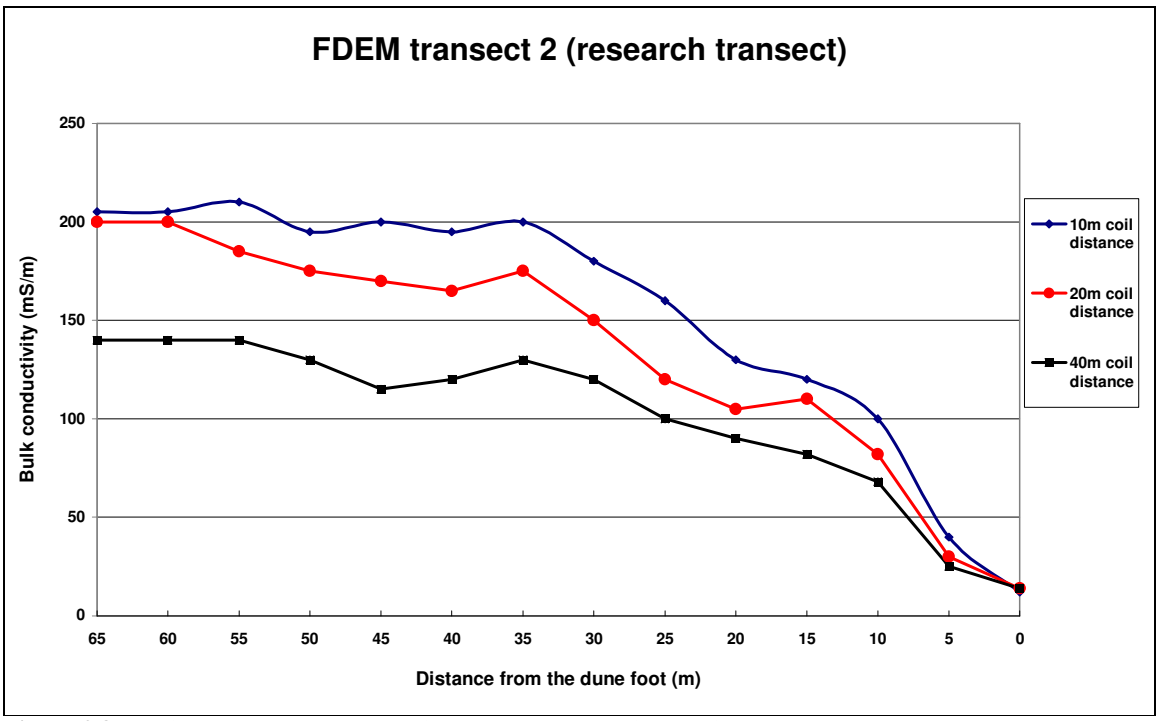

Figure 3.8 *Results of the FDEM survey along transect 2, which is on the research transect, for each coil distance.*

Small differences in apparent resistivity values are observed between '4200' and '4400', for the 10m coil distance (Figure 3.5). A decline of the apparent resistivity values occurs from 35m from the dunefoot. At 10m from the dunefoot, apparent resistivity values sharply drop from a value around 100 mS/cm to around 20 mS/cm. The 20m coil distance (Figure 3.6), indicates significant differences between the two profiles, where apparent resistivity values at '4200' are lower than at the '4400' transect. At 10m from the dunefoot, the differences become small

again. The observed differences at the 20m coil spacing are even more pronounced at the 40m coil spacing (Figure 3.7).
Figure 3.8 depicts the results for the three coil distances on transect 2, which was located on the research transect. Here, the presence of less saline water beneath salt water is again indicated by the decrease in bulk conductivity with an increasing penetration depth (coil distance).

3.3.2 VES measurements

For the model interpretation, the formation factor was estimated at 5 and the EC (non-specific EC) of seawater was estimated at 35 mS/cm. The formation factor is rather high, but had to be used to obtain a proper model fit of the VES (Figures 3.9 and 3.10). From equations 3.2 and 3.3, the specific resistivity of sediment layers containing fresh, brackish and salt water were calculated at respectively 100, 15 and 1.5 Ωm. The model interpretation is arbitrary in some degree, because VES measurements are often accompanied by equivalence problems. The specific resistivity values for the fresh, brackish and salt layer are therefore kept constant for the model interpretation of the two VES measurements, in order to let the layer thickness vary. However, extra layers had to be inserted to obtain a proper fit.
The resulting layer model for VES 1 is shown in Figure 3.9 and Table 3.1. The depth of the salt-brackish groundwater interface is modeled at 10m from the surface. Fresh groundwater layer is modeled from 10 to 70m depth. Again, a sharp interface is used to model the fresh-salt groundwater interface.

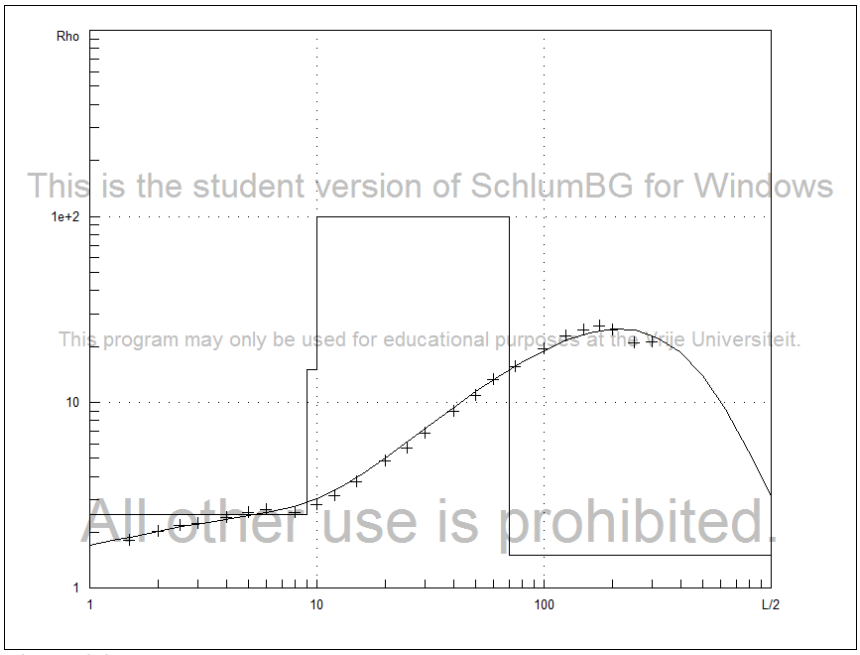

Figure 3.9 *Interpretation of VES 1 using the SchlumBG program.*

Table 3.1 *Layer model for VES 1*

Resistivity (Ω m)	Depth (m from the surface)
1.5	0.6
2.5	9
15	10
100	70
1.5	-

The results for VES 2 are given in Figure 3.10 and Table 3.2. The depth of the salt-brackish groundwater interface is modeled at 5m depth. The brackish-fresh groundwater interface is modeled at 8m depth. The fresh groundwater layer extents to 68m from the surface. A sharp interface is used to fit the model data for the deep fresh-salt groundwater interface.

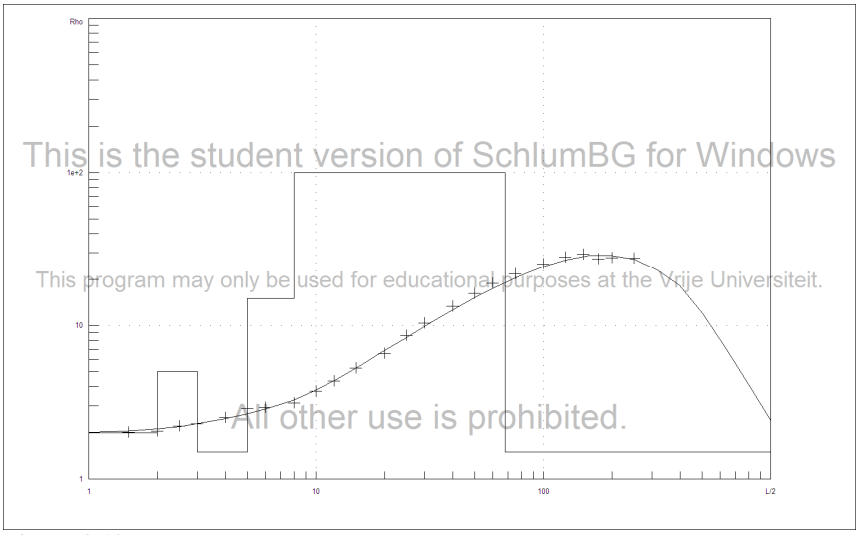

Figure 3.10 *Interpretation of VES 2 using the SchlumBG program.*

Table 3.2 *Layer model for VES 2*

Resistivity (Ωm)	Depth (m from the surface)
2	2
5	3
1.5	5
15	8
100	68
1.5	-

3.3.3 CVES measurements

Results of the interpretation of the three CVES measurements orientated perpendicular to the shoreline are shown in Figures 3.11-3.13. The high water line was situated at approximately 20m east from the centre of the profile, where east is the right side in Figures 3.11-3.13. Here, mixing of fresh and salt water occurs. East of this zone, lower resistivities are observed near the surface. The electrodes were placed 0.5m deeper in the sand here, to cope with possible contact problems (Figure 3.4). In this way, all electrodes were in close contact (<0.5m) with the groundwater table.
A wedge shape distribution of salt groundwater is observed in each figure, where the depth of the salt-brackish interface (3 Ωm) increases toward the low water line. A slight alongshore trend is observed, where the salt-brackish and the brackish-fresh groundwater interfaces (15 Ωm) increase to the north.
Because the specific resistivity is inversely proportional to pore water EC (eq. 3.2 and 3.3), small variations in specific resistivity correspond with a large range in EC. Subtle variations in the salt water wedge in Figures 3.11 – 3.13 indicate possible mixing of salt and fresh water in the 'salt wedge'. These possible mixing processes will be further discussed in section 3.3.6.

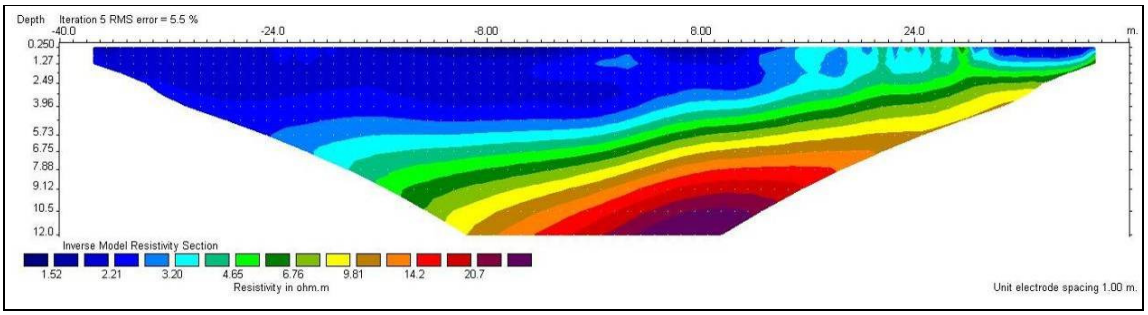

Figure 3.11 *Interpretation of CVES 1, measured at the research transect.*

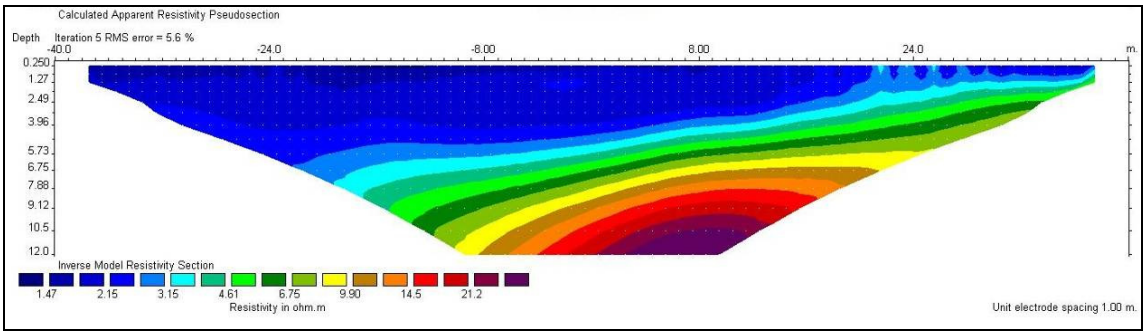

Figure 3.12 *Interpretation of CVES 2, measured 50m north of the research transect.*

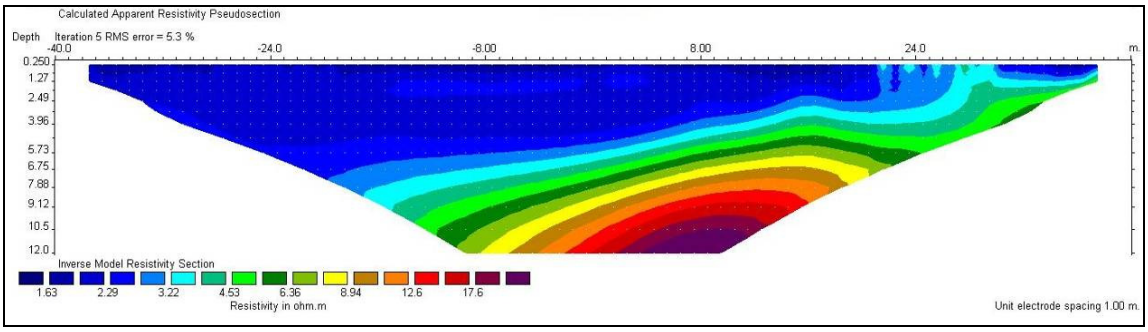

Figure 3.13 *Interpretation of CVES 3, measured 100m north of the research transect.*

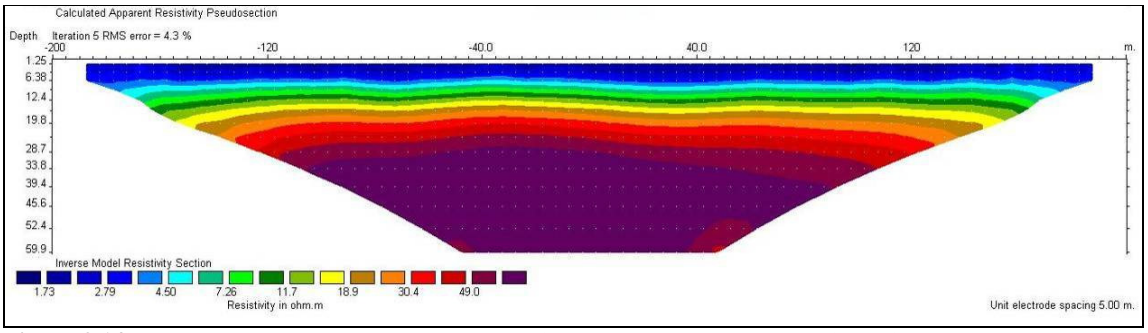

Figure 3.14 *Interpretation of CVES 4, located at the low water line and orientated parallel to the shoreline. Profile length amounts 400m, which resulted in a measurement depth of 60m.*

Figure 3.14 shows the interpretation of CVES 4, which was orientated along the shore at the low water line. The horizontal axis is positive northward. The research transect is located in the centre of this CVES measurement.
The brackish-salt interface varies between 6 and 8m depth along the profile. This is comparable with the shore-perpendicular observations. The brackish-salt interface varies between 12 and 20m depth, where its depth somewhat increases north of the research transect. Fresh groundwater is located below this interface and extents to at least 60m -MSL.

3.3.4 TDEM soundings

TDEM soundings 1 and 2 were performed near each other in the valley east of the foredune ridge (Figure 3.2). The fresh-salt groundwater interface of TDEM sounding 1 is modeled at approximately 86m from the surface, which is about 82 –MSL. TDEM sounding 2 indicates that the fresh-salt groundwater interface is located at 90m from the surface, which corresponds to a comparable relative depth as TDEM sounding 1.
TDEM sounding 3 is located near the groundwater divide. The fresh-salt groundwater interface is located at 95m from the surface here, which corresponds to 90m –MSL. TDEM sounding 4 was located at the beach, near the dunefoot. Results of this sounding are poor because the resistivity variation is too high in the subsurface of the sampled area. This sounding is therefore not discussed.

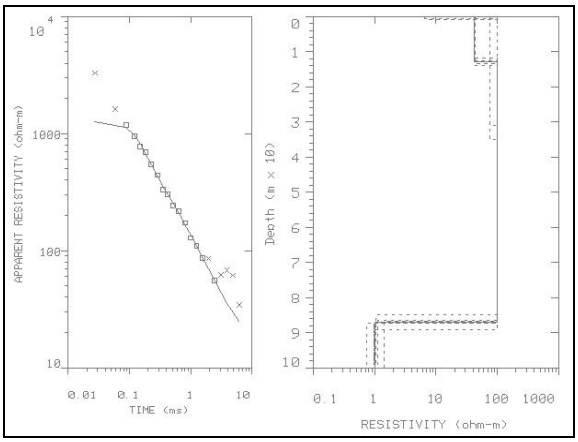

Figure 3.15 *TDEM sounding 1*

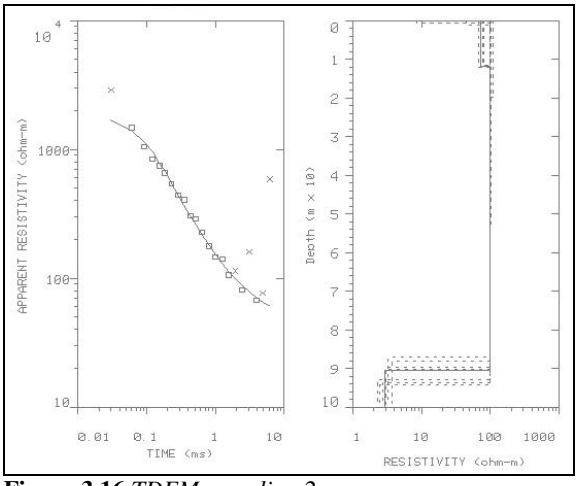

Figure 3.16 *TDEM sounding 2*

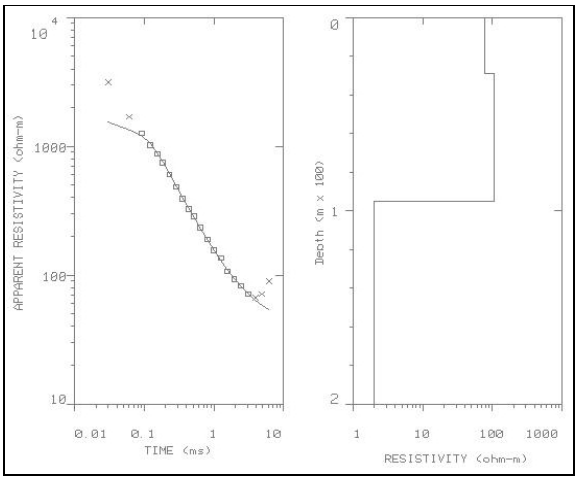

Figure 3.17 *TDEM sounding 3*

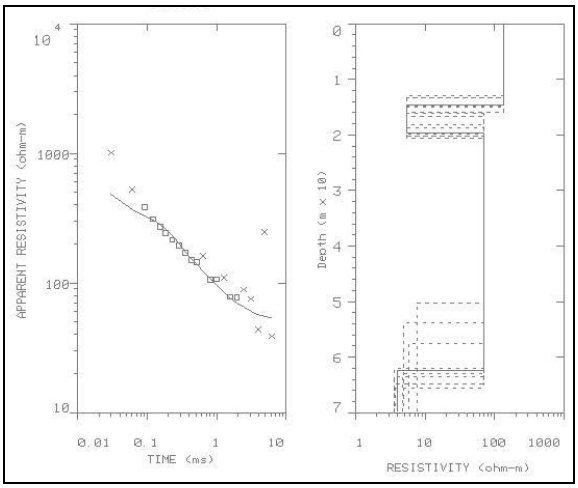

Figure 3.18 *TDEM sounding 4*

3.3.5 Water table measurements

Results of the water table measurements performed in January and September are shown in Figure 3.19. The groundwater table was 0.6-0.7m higher in January due to higher rainfall and lower evaporation. The hydraulic gradient is around 0.003 near the groundwater divide. Close to the sea, the hydraulic gradient increases to 0.007.

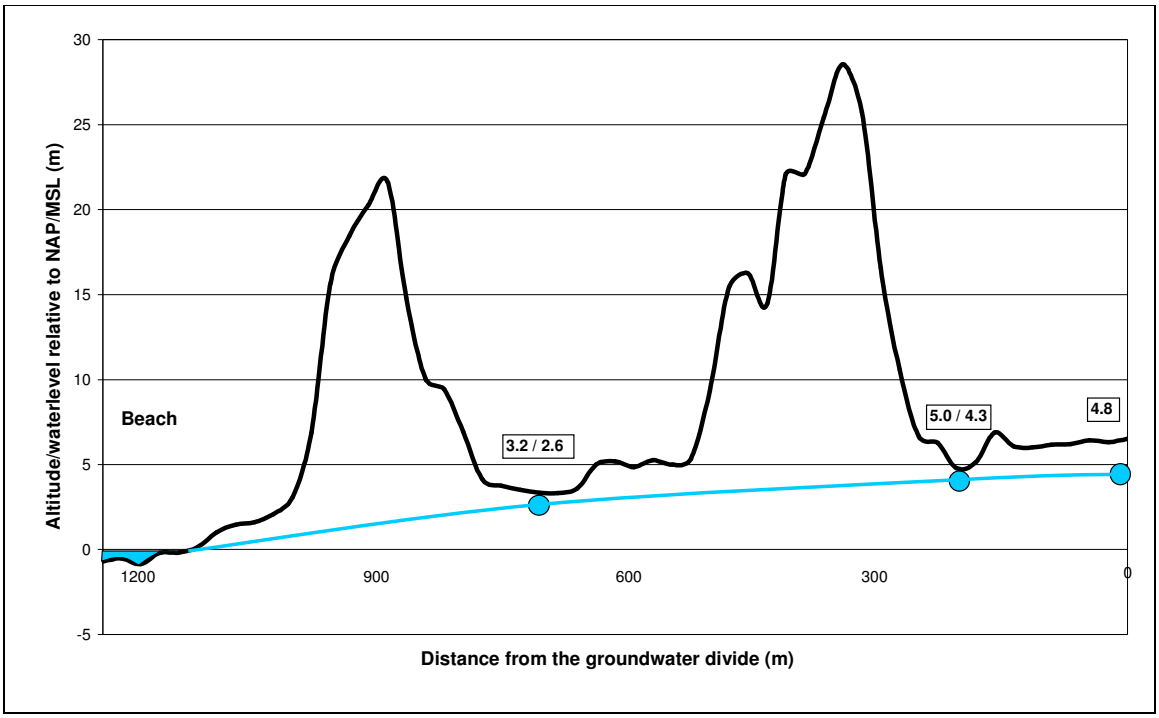

Figure 3.19 *Sketch of the water table measurements (in m) and an interpolation hereof along the research transect. The reference height is the NAP. Measurements including a dash indicate the height of the groundwater table in January 2009 (left) and September (right). The water table measurement near the groundwater divide was only measured in September.*

3.3.6 CTD diver measurements

Figure 3.20 depicts the position of the groundwater table relative to the beach surface. By choosing the beach surface as a reference, beach draining above the diver can be observed. This was relevant for deducing a boundary condition for the numerical model (section 4.2.2). Near the low water line (location 'Low water line'), the 'groundwater' level approximately corresponds to the sea level and shows the highest variation. Even when the beach is inundated by the sea, the groundwater level variation decreases in the direction of the dunes. This is caused by the hydraulic conductivity of the beach sediment, which is also responsible for the reduced slope of the groundwater level during falling tide. The time series starts three days after spring tide and ends around spring tide again. It is therefore expected that the tidal amplitudes first decrease and then increase. This is however not clearly observed in figure 3.20, because wind and the related sea swell have a profound impact on the sea level, tidal zone extension at the beach and therefore also the groundwater level at the beach. Strong southwesterly wind on September 3, 4 and 5 was for instance responsible for the high water levels on these days.
Figure 3.21 depicts the temperature of the groundwater at the three measurement locations. Locations 'Middle' and 'High water line' show a gradual decline in temperature. Diurnal and daily patterns are not observed. These patterns match with the sea water temperature pattern for this period. This means that the travel time from infiltrating seawater to the diver location is relatively small and that seawater infiltration occurs at the beach.
A gradual increase in temperature is observed at location 'Low water line', opposite to the air (Figure 3.22) and seawater (Figure 3.23) temperature pattern for the measurement period. The temperature at the beginning of the measurement period was around 16.5 ^{o}C, about 5^{o}C lower than the temperature of the sea. The observed pattern is thought to reflect the temperature

pattern of former (colder) infiltrated seawater. Downward vertical flow and seawater infiltration near this location is however significantly less than at locations 'High water line' and 'Middle', because it would otherwise show a comparable, decreasing temperature pattern. Small vertical movement of the groundwater at this location can however occur. This is indicated by the diurnal patterns in temperature between 29-8 and 3-9. During eb tide, the groundwater temperature decreases. This is caused by upward vertical flow transferring relatively colder groundwater upward. During flood, the groundwater temperature increases, indicating downward vertical flow. During periods of higher groundwater levels, as at 3-6 September, temperatures seem to stabilize. This suggests that the groundwater flow velocity at this location decreases due to the elevated sealevel.

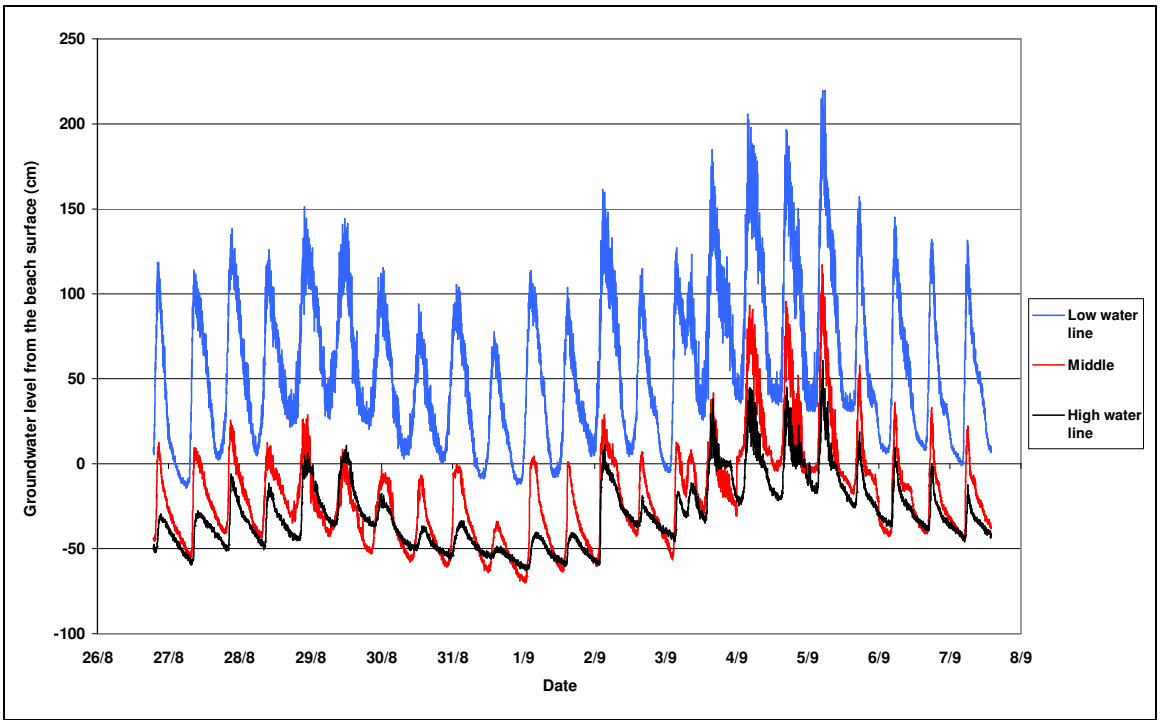

Figure 3.20 *Groundwater levels in cm from the beach surface. The labels 'Low water line', 'Middle' and 'High water line' refer to the location at the beach (section 3.2.6). Note that the groundwater is relative to the beach surface.*

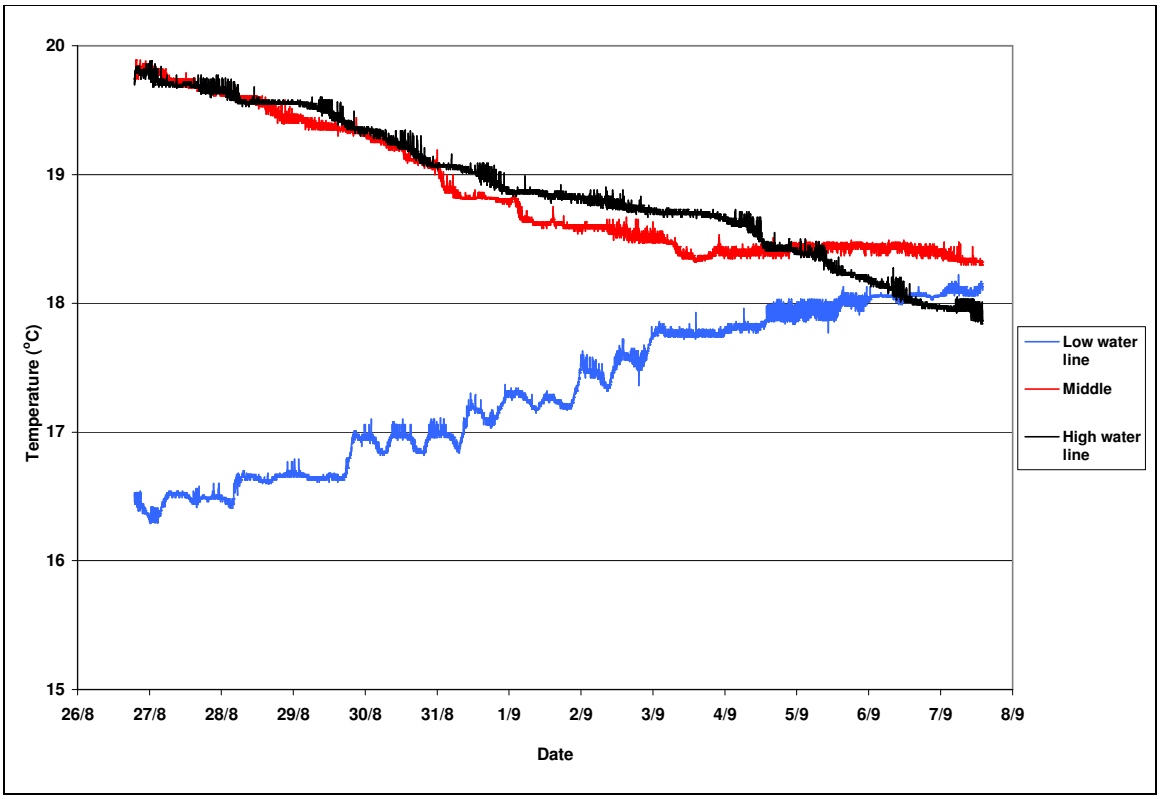

Figure 3.21 *Groundwater temperature at the three measurement locations.*

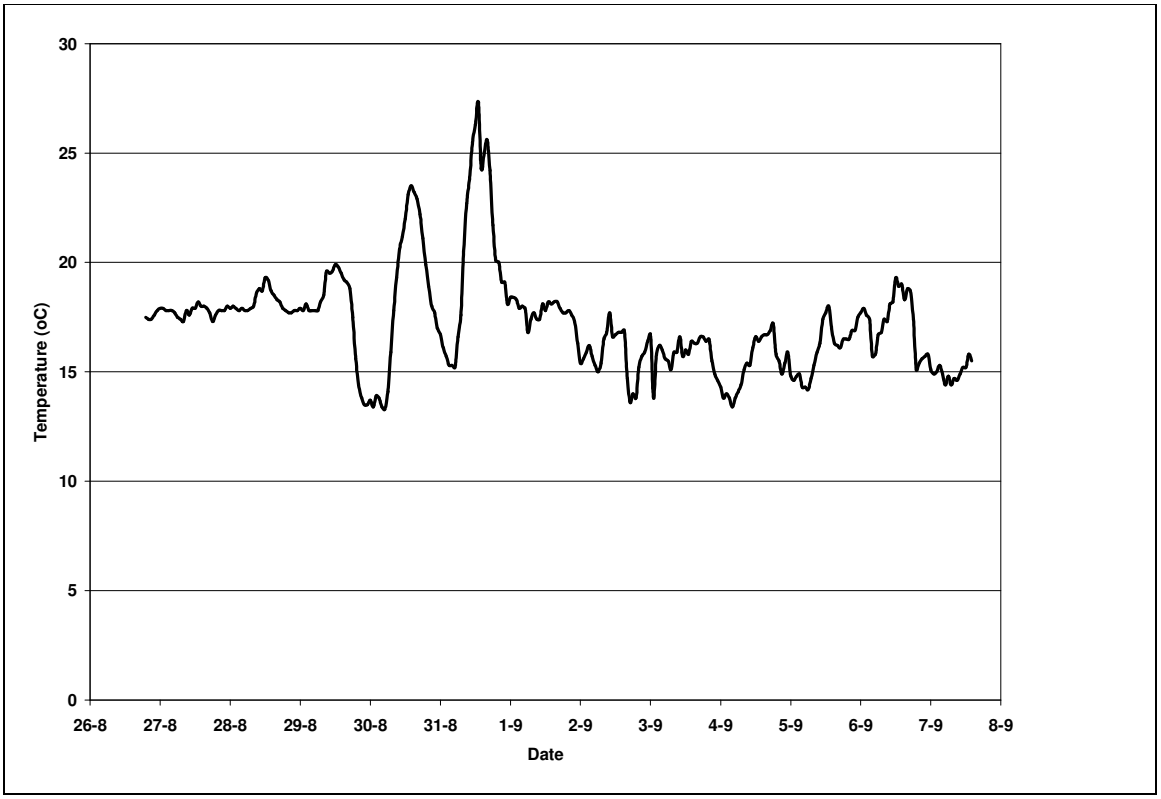

Figure 3.22 *Air temperature measured at Wijk aan Zee, a weather station about 10km south of the research transect (KNMI, 2009b)*

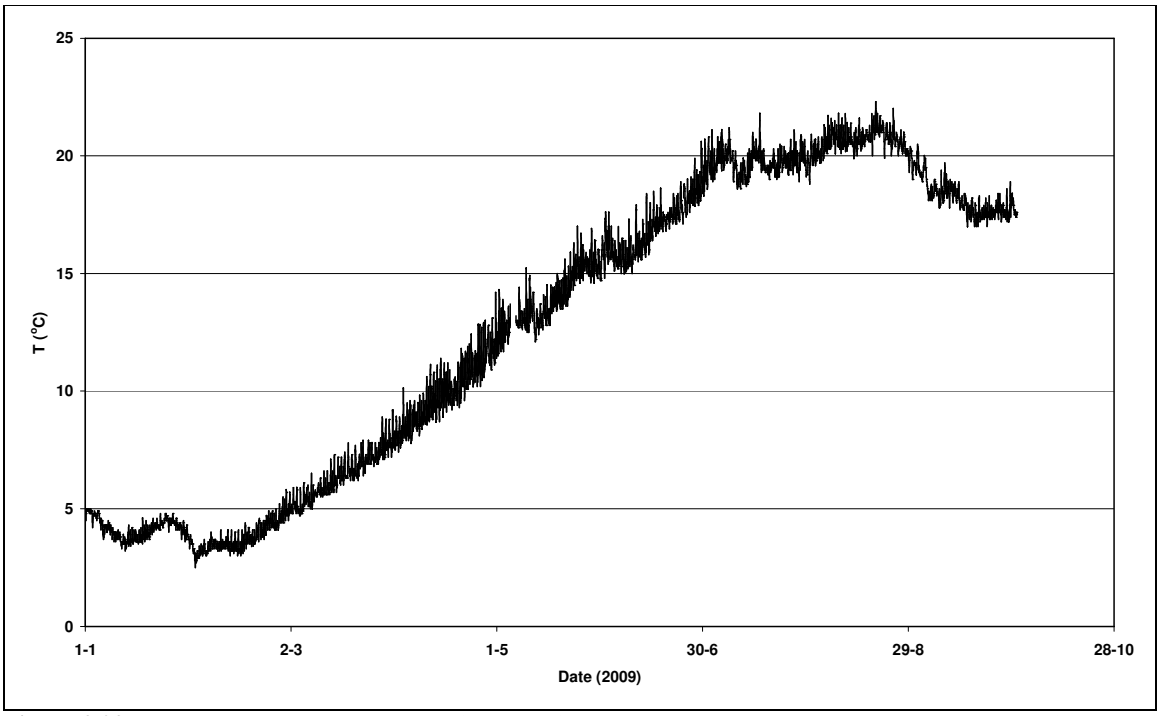

Figure 3.23 *Sea water temperature measured at Ijmuiden Buitenhaven, a marine measurement station about 15km south of the research transect (Rijkswaterstaat, 2009).*

The specific EC of the groundwater at the three measurement locations for the measurement period is shown in Figure 3.24. At location 'Middle', the EC is relatively stable. The same holds for location 'Low water line', although a decreasing trend is observed from 30-8 to 2-9. This could be caused by upward flow of less saline groundwater which was favored by the relatively low sea levels during these days.
The specific EC at location 'High water line' is more fluctuating. Flow of salt water from the sea and freshwater from precipitation and the dune area have resulted in the observed complex pattern. The decreasing trend from 2-9 to 9-8 is contradictory with the groundwater levels on these days, which were elevated due to a storm event. Most likely, precipitation on these days caused the EC to decrease.

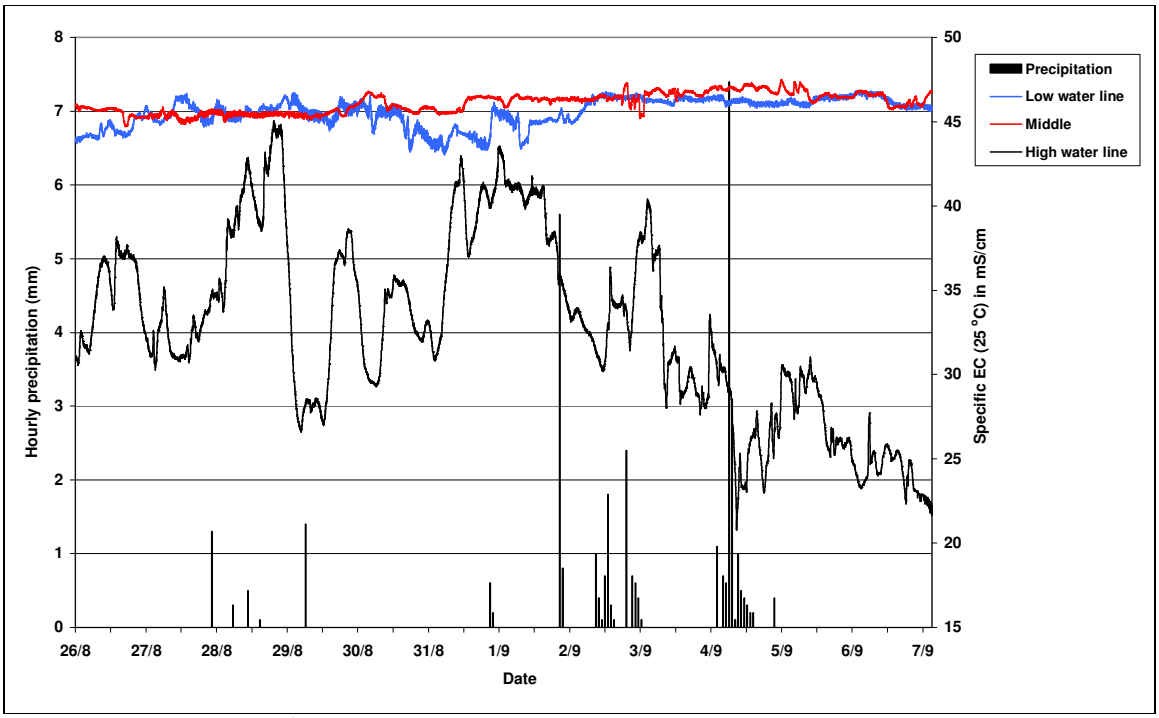

Figure 3.24 *Specific EC (25°C) and hourly precipitation (KNMI, 2009b) from 26/08/09 – 07/09/09.*

3.3.7 Groundwater salinity distribution along the research transect

The groundwater table and the location of the deep fresh-salt groundwater interface along the research transect, deduced from the VES and TDEM measurements, are shown in figure 3.25. Near the groundwater divide, the interface is at -90m MSL. The groundwater table and the depth of the interface decrease in the direction of the sea. At the beach, the interface is at approximately -70m MSL. As has been described in section 3.3.5, the gradient of the phreatic level is not equal along the research transect. The same holds for the depth of the fresh-salt groundwater interface, which decreases stronger in the vicinity of the beach. In the intertidal zone, fresh groundwater recharge from precipitation is relatively small compared to seawater infiltration. When it is assumed that the current hydrological boundary conditions are responsible for the observed fresh-salt groundwater interface, the depth of this interface at the beach can only be explained by the flow of fresh water toward the sea. This will be further discussed in chapter 5. The interface is assumed to be sharp and relatively stable over time, as pumping activities have a minor impact (section 2.4).
Figure 3.26 shows an interpolation of the more shallow salt-brackish and the brackish-fresh groundwater interface at the beach along the research transect, deduced from the geophysical measurements. These interfaces are thought be more dynamic than the deep fresh-salt groundwater interface due to the tide, weather and groundwater flow from the dune area (seasonal change). The 'high water line' diver revealed significant salinity changes over a period of 12 days, which suggests that the salt-brackish groundwater interface is indeed dynamic.
The salt-brackish groundwater interface in the intertidal area was largely deduced from CVES 1, using the 3 Ωm contour level. Near the low water line, CVES 4 was used for this. The VES measurements were not used for this interface, because of the uncertainties that arise in the model interpretation by equivalence problems (section 3.3.2).

The brackish-fresh groundwater interface was deduced from CVES 1 and 4, VES 1 and 2 and the FDEM survey. Because the interface is deeper than the salt-brackish groundwater interface, it is assumed to vary less in time.

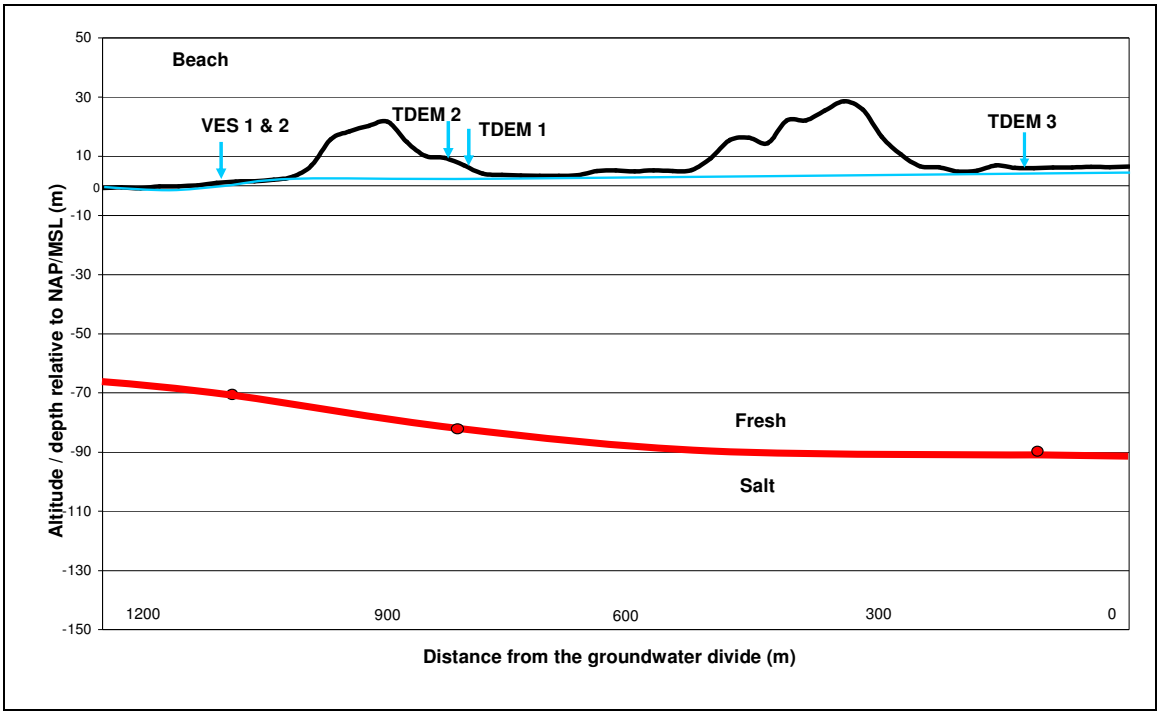

Figure 3.25 *Interpolation of the depth of the deep fresh-salt groundwater interface(in red) and the phreatic level (in blue) along the research transect, deduced from field observations. The interface is assumed to be sharp.*

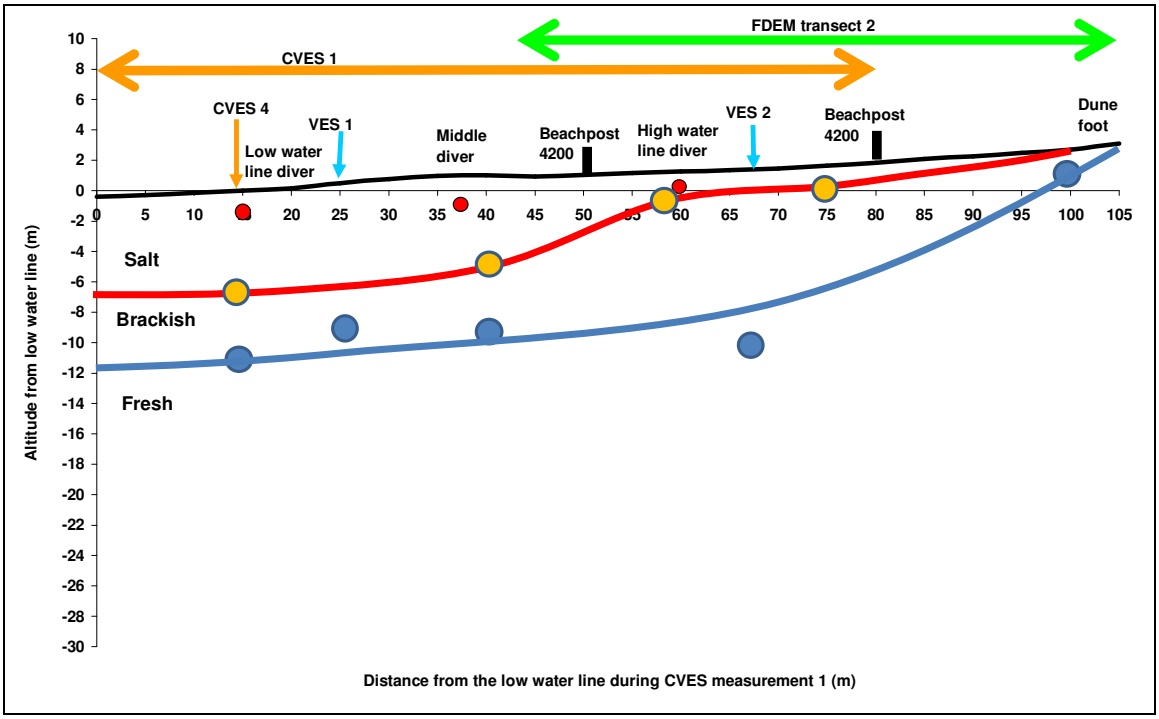

Figure 3.26 *Interpolation of the depth of salt-brackish (in red) and brackish-fresh (in blue) groundwater interface at the beach along the research transect, deduced from geophysical measurements.*

4 Numerical groundwater flow modeling

4.1 Introduction

2D numerical models were used to simulate the evolution of a freshwater lens and fresh groundwater flow to the sea, starting with saltwater conditions and neglecting alongshore groundwater flow.
As is already mentioned, the formation of a submarine fresh groundwater tongue is expected when low permeable sediments are present in the subsurface. In addition, they influence the near-shore salinity distribution, as will be further elucidated in chapter 5. While onshore data is abundant, offshore geological data was not available. Several model simulations were therefore performed using different hydrogeological parameterizations.

4.2 Methods

4.2.1 Description of the used code: SEAWAT 2000

Where significant variations in fluid density are present, like in coastal aquifers, groundwater flow and fluid density are coupled. The SEAWAT 2000 code (Guo and Langevin, 2002) has been used to simulate the variable density groundwater flow. SEAWAT 2000 combines the groundwater flow code MODFLOW 2000 (Harbaugh et al., 2000) and the solute transport code MT3DMS (Zheng and Wang, 1999). The MODFLOW and MT3DMS input files were made using the software Processing Modflow for Windows pro (PMWIN pro; Chiang, 2005).
The flow equation is based on the concept of freshwater head. The resulting governing partial differential equation for density dependent groundwater flow used by SEAWAT 2000 is:

$$\nabla \cdot \left[\rho \, K_f \left(\nabla h_f + \frac{\rho - \rho_f}{\rho} \cdot \nabla z \right) \right] = \rho \, S_f \frac{\delta h_f}{\delta t} + n_e \frac{\delta \rho}{\delta t} - \rho_s q_s$$

where:
ρ [M L^{-3}]= the fluid density,
K_f [L T^{-1}] = the equivalent freshwater hydraulic conductivity,
h_f [L] = the equivalent freshwater head,
ρ_f [M L^{-3}]= the freshwater density,
z [L] = the vertical coordinate, with z = 0 at MSL and negative in the downward direction,
S_f [L^{-1}] = the equivalent freshwater storage coefficient,
t [T] = the time,
n_e [-] = the effective porosity,
ρ_s [M L^{-3}]= the density of fluid source,
q_s [T^{-1}] = the flow rate per unit volume of aquifer of the fluid source or sink.

The Preconditioned Conjugated Gradient (PCG) package is used to solve this density dependent groundwater flow equation.

The governing equation for the solute transport is:

$$\frac{\delta(n_e C^k)}{\delta t} = \nabla \cdot (n_e D \nabla C^k) - \nabla \cdot (n_e \vec{v} C^k) - q_s C_s^k$$

where:

C^k [M L^{-3}]= the concentration of dissolved species k,
D [L^2 T^{-1}]= the hydrodynamic dispersion tensor,
$\vec{v}$ [L T^{-1}] = the linear pore water velocity and
C_s^k [M L^3] = is the concentration of species k from the source/sink.

The advection term, $-\nabla \cdot (n_e \vec{v} C^k)$, of this equation is solved using the Eulerian Lagrangian method Hybrid Method of Characteristics (HMOC). This scheme is able to switch between the Method of Characteristics (MOC) scheme and the Modified Method of Characteristics (MMOC) scheme. The MOC scheme is used where sharp concentration fronts are present, because this scheme is virtually free of numerical dispersion. The main drawback of this scheme is the large computational efforts that are required, especially when a large number of particles are used. The MMOC scheme makes use of only one particle and is therefore less memory demanding and somewhat faster than the MOC scheme. Away from the sharp concentration fronts, this scheme is applied. Table 4.1 shows an overview of the different parameters used in the MMOC scheme.

Table 4.1 *Parameter values used in the MMOC scheme. MXPART is the maximum number of particles used, PERCEL is the Courant number, WD is the concentration weighting factor, DCEPS is the criterion for placing particles, NPLANE is a flag which indicates whether a fixed or random pattern is used for the initial placement of the particles, NPL and NPH control the number of initial particles placed per cell depending on the concentration gradient, NPMIN is the minimum number of particles allowed per cell, NPMAX is the maximum number of particles allowed per cell, NLSINK is a flag which indicates whether a fixed or random pattern is used for the initial placement of the particles to approximate sinks cells in the MMOC scheme, NPSINK is the number of particles used to approximate sink cells in the MMOC scheme and DCHMOC controls the switch between the MMOC and MOC scheme by a critical relative concentration gradient.*

Parameter	Value
MXPART	800000
PERCEL	0.75
WD	0.5
DCEPS	0.00001
NPL	10
NPH	40
NLSINK	0
NPSINK	15
DCHMOC	0.001

A finite difference method is applied to solve the dispersion, sink/source and reaction term, using the Generalised Conjugated Gradient Solver (GCG) package.
Concentration and fluid density are related by the following equation:

$$\rho = \rho_f + \frac{\delta \rho}{\delta C} C$$

where C is the concentration of the solute.
For this study the solute concentration varies between 1 (salt water) and 0 (fresh water). For salt water, a density of 1023 kg/m^3 is assumed, while the density of freshwater is assumed to be 1000 kg/m^3. The flow and transport equations are explicitly coupled, using the concentrations from the previous time step to calculate fluid densities.

Although SEAWAT 2000 uses the concept of equivalent freshwater head, parameters in the input and output files are written as native aquifer heads.
To visualize the concentration output file, a Python (Python, 2009) script was used, constructed by Vincent Post.

4.2.2 Model design and boundary conditions

The formation time of a freshwater lens in the coastal dune area of the Netherlands, starting from salt water conditions, is in the order of centuries (Stuyfzand, 1993). Annual rainfall, sea level, land and sea bottom elevation and the position of the shoreline have changed during the past few centuries. This has not been taken into account in the model simulations. Land and sea bottom elevation changes were neglected, while the position of the shoreline remained stagnant over the simulation time. Annual rainfall and sea level were implemented using stationary boundary conditions. Sea water infiltration at the beach driven by the (diurnal) changing sea level has been using a non-tidal boundary condition, which was deduced from the CTD diver observations (section 3.3.6). This will be further explained at the end of this section.
The horizontal extent of the model is 4000m, subdivided in 400 columns. The left 1250m of the model represents the research transect. The position of the right side of the model was arbitrary chosen at 4000m from the groundwater divide, in order to simulate the development of a fresh, submarine groundwater tongue. The top of the model coincides with the NAP and mean sea level. 75 layers have been used for the 150m vertical extent. The grid cell size is constant in the model, so every cell is 10m by 2m. The longitudinal dispersivity is set to 0.1m. Although a Péclet criterion ≤ 2 is generally recommended in literature to minimize numerical dispersion and artificial oscillation, this condition is not applied in the model because of the high computational efforts it would require in this study. The HMOC scheme is therefore used to minimize these errors. Similar approaches were applied in other numerical studies of variable density groundwater flow on comparable spatial and temporal scales (Vandenbohede and Lebbe, 2006, Kuiper, 2007).
On the left, bottom and right side of the model, no-flow boundaries are applied. The left side represents the groundwater divide in the dune area. The flow of the deep salt water below the freshwater lens toward the polder areas has been neglected because the flow rate is relatively low (< 20m/yr (Oude Essink, 1996)).

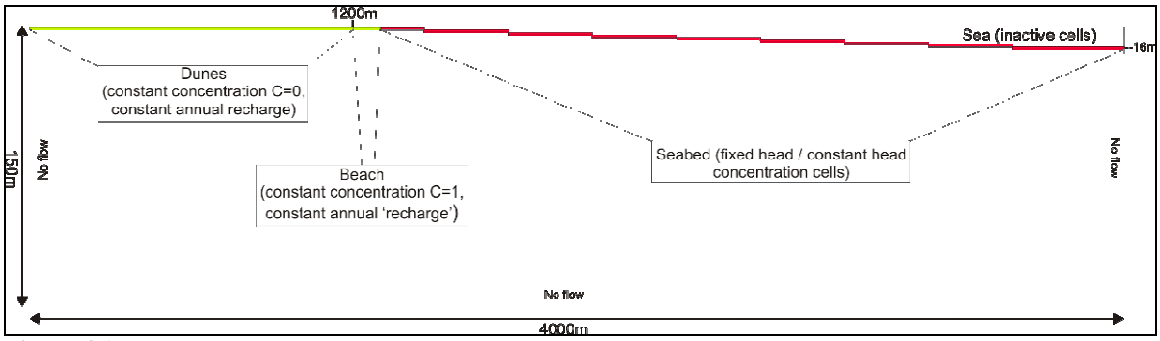

Figure 4.1 *Overview of the applied boundary conditions in all numerical model simulations. The active cells are bordered by three no flow boundaries, one defined flow boundary (well function, shown in green) and one fixed head boundary (IBOUND package (MODFLOW), shown in red). A zero concentration is applied for recharge from the dune area, whereas at the beach seawater infiltration is simulated with a fixed concentration of 1. The green zone enclosing well function cells is exaggerated, where only the upper cells are defined with the well package. Numbers outside the model domain indicate distance and length in meters. Note that this model is mirrored compared to the field measurement results.*

Table 4.2 *Input values for the Well package (MODFLOW) in cells 121-125 in layer 1, to simulate seawater infiltration at the beach.*

Dunes						**Sea**
Model cell nr.	121	122	123	124	125	
Recharge in $m^3\ m^{-2}\ yr^{-1}$	139	320	500	250	0	

The top layer of the model contains three different boundary conditions. A constant flux boundary condition is applied to columns 1-120 with a constant concentration of 0, to simulate the recharge of the groundwater system. The Well package is used with a recharge rate of 350mm per year.
Salt water infiltration on the beach, driven by the diurnal changing sea level, is simulated in columns 121-125. Again, the Well package is used but with a constant concentration of 1. The amount of 'recharge' and the average length of the seawater infiltration zone was estimated from the water level measurements by the CTD divers (section 3.3.6). For the measurement period, the total volume of seawater that was able to infiltrate was calculated (Figure 4.2). First, the minimum groundwater level for each tidal cycle was determined. From this, the volume from the groundwater table to the beach surface was determined. Only when the beach above the diver was actually inundated by the sea, this volume was taken into account. Inundation above the diver could be deduced from figure 3.20. The height of the capillary fringe (h_c) was then calculated from:

$$h_c = \frac{2\ \sigma}{\rho\ g\ r},$$

where σ is the surface tension, ρ is the density of the pore water, g is the gravitational acceleration and r is the effective pore diameter. Assuming a pore water temperature of 20°C (resulting in a surface tension of 0.0727 N m^{-1}), a pore water density of 1023 kg m^{-3}, a gravitational acceleration constant of 9.81 and an effective pore diameter of 300 µm (coarse sand), the resulting height of the capillary fringe is 0.05m. For the volume on top of the capillary fringe it was assumed that the beach has drained until field capacity (pF of 2.0), where field capacity was estimated at 10% volumetric water content (θ). Last, the porosity (n) of the beach sediment was estimated at 0.3.

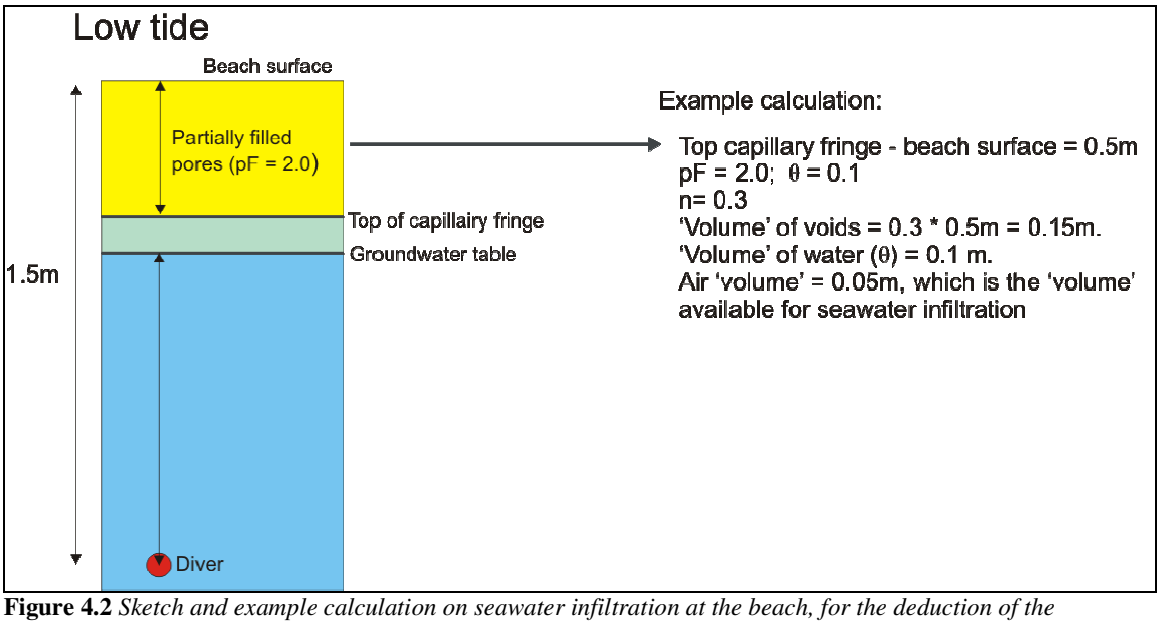

Figure 4.2 *Sketch and example calculation on seawater infiltration at the beach, for the deduction of the boundary condition at the beach.*

The total volume available for seawater infiltration over the measurement period was then calculated and extrapolated to a yearly amount. The measurement period has thus been regarded as representative for a year. The input values for cells 121, 123 and 125 (Table 4.2) were deduced from the CTD diver measurements, while cells 122 and 124 have been linearly interpolated by taking the mean of the adjacent cells. The vertical inflow of seawater due to increase of the hydraulic gradient by elevated sealevels above the beach surface is neglected. This holds mainly for the two cells near the sea, as can be deduced from Figure 3.20. However, groundwater temperature data from the CTD diver near the low water line indicated that seawater infiltration is relatively low here. The cells which represent the area around the high water line are less affected by the assumption, because the sea rarely rose higher than the beach level there (Figure 3.20).
Table 4.2 shows the resulting input values for the Well package. In this way, sea water infiltration at the beach is directly modeled, while this can also be modeled indirectly using a tidal boundary condition. The computational efforts for the numerical simulations including a tidal boundary condition of this timescale are however unrealistic. Furthermore, a tidal boundary condition where the influence of wind and sea swell on sea level is neglected is probably a too simplified approach to simulate the salt and fresh groundwater dynamics at the beach of the research transect. Long term on site water level data as input for sea water level could be an alternative.
The elevation of the seabed has been incorporated in the model. This was deduced from elevation data from a topographic map (Wolters-Noordhoff, 1988). The seabed, located in columns 126-400, encloses fixed head cells having a hydraulic head of 0 and a solute concentration of 1. Water and solute is thus allowed to transfer over this boundary depending on the hydraulic heads in layer 2.
The model simulation time is 1000 years, subdivided over 500 time steps. The boundary conditions remain constant throughout the total simulation time. The amount of transport steps are restricted to criteria defined within the HMOC scheme (table 4.1).

4.2.3 Model parameters

The sedimentary deposits along the research transect were subdivided in several hydrogeological units. The porosity and the specific storage were assumed to be constant along the profile. The longitudinal, horizontal transverse and vertical transverse dispersivity for all units were chosen to relative small values of 0.1m, 0.01m and 0.01m respectively (after: Oude Essink, 1996). Table 4.4 depicts and overview.
Several units enclose more than one sediment class. In order to obtain a representative vertical (K_v) and horizontal (K_h) conductivity of these units, the following formulae were used:

$$K_h = \sum k_i \left(\frac{b_t}{b_i} \right) \quad (4.1) \quad \text{and} \quad K_v = \frac{b_t}{\sum \frac{b_t}{k_i}} \quad (4.2)$$

The calculated difference between the horizontal and vertical hydraulic conductivity was found to be small (<2). The hydraulic conductivity of all hydrogeological units was therefore regarded as isotropic.
For the ‘Holocene’ and ‘Pleistocene’ units, borehole data of B19C390 and B152 from Dinoloket (Dinoloket, 2009) were used to calculate the horizontal and vertical hydraulic conductivity. To each sediment class (Table 4.3), a hydraulic conductivity was assigned. The small loam layer present in borehole B152 was not included in these units, but was defined separately (the ‘Loam’ unit). Because the cells are 2m in the vertical, a representative vertical

hydraulic conductivity was calculated using equation 4.2, including a 1.85m layer of medium fine sand.
The 'Beach' unit was defined because coarse sediment is found on the beach (Pieterse, 2009, Biewinga et al., 1991).
The 'Till and Clay' unit encloses glacial till of the Drenthe formation and low permeable sediments from the Eemian formation. The vertical hydraulic conductivity of the glacial till was derived from Stuyfzand (1993). Equation 4.2 was used to calculate a representative vertical hydraulic conductivity for the low permeable sediments of the Eem formation, again using data from borehole B152. The vertical hydraulic conductivity of these units were comparable, which is the reason why these sediments have been combined in one unit.
The unit 'Bottom sands' represents the Urk, Sterksel and Appelscha formations. The hydraulic conductivity of these units was estimated from Stuyfzand (1993). The thin clay layer indicated in borehole B152 was neglected here.
The distribution of these units was based on data from Stuyfzand (1993) and the hydrogeological profiles shown in Appendix B and C. Four numerical simulations have been performed using different distributions of the 'Loam' and 'Till & Clay' units, to investigate their influence on the formation of fresh, submarine tongues and groundwater salinity distribution. In simulation 1, both units are present and are assumed to continue offshore. In simulation 2, the 'Loam' unit is neglected and therefore not incorporated. This simulation was performed to study the effect on neglecting thin resistant layers in the subsurface. In simulation 3, the 'Loam' unit is extending only 200m offshore to study the effect of the extension of thin resistant layer offshore. In simulation 4, both resistant units are not present. This simulation aims to give insight in fresh groundwater flow towards the sea in a situation where resistant layers are absent. Figures 4.3-4.6 depict a sketch of these different hydrogeological configurations from the groundwater divide (left) to 300m west of the beach (right). The colors correspond to the colored hydrogeological units and their parameters shown in table 4.4. Because relevant geological data was not available, the configurations at the right side in figures 4.3 – 4.6 have been extended to 4000m from the groundwater divide without modifications.

Table 4.3 *Assigned hydraulic conductivity values to the sediment classes in boreholes B152 and B19C390.*

Sediment class	Hydraulic conductivity K, in [m d^{-1}]
Loam and clay	0.001
Fine sand	1
Medium fine sand	5
Medium coarse sand	20
Coarse sand	40

Table 4.4 *Overview of the hydrogeological units and their parameter values applied in the model. Colors correspond to the colored hydrogeological units in figures 4.3-4.6. Values for hydraulic conductivity (K), porosity (n) and storage coefficient (S) are based on data from Stuyfzand (1993) and Domenico and Schwarz (1990).*

Unit name	Material	Lithostratigraphic units	K [m d^{-1}]	n [-]	S [-]
Beach	Coarse sands	Recent deposits	40	0.30	10^{-4}
Holocene	Medium sands, fine, silty to clayey sands	Naaldwijk and Nieuwkoop formations.	2	0.30	10^{-4}
Loam	Silty loam	Krefteheye formation (?)	0.01	0.30	10^{-4}
Pleistocene	Fine, medium and coarse sands, clay and loam.	Kreftenheye and Eem formations.	4	0.30	10^{-4}
Till & Clay	Glacial till and marine clay	Eem and Drenthe formations	0.002	0.30	10^{-4}
Bottom sands	Medium and coarse sands	Urk, Sterksel and Appelscha formations	25	0.30	10^{-4}

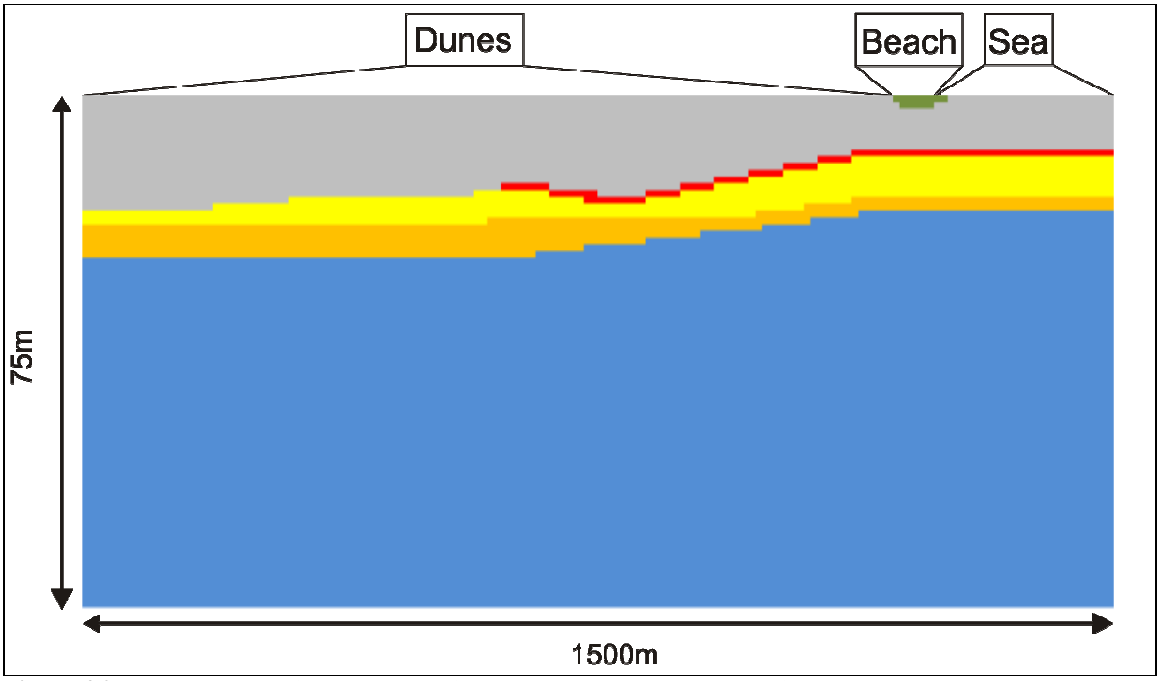

Figure 4.3 *Configuration of hydrogeological units applied in simulation 1. All units are present.*

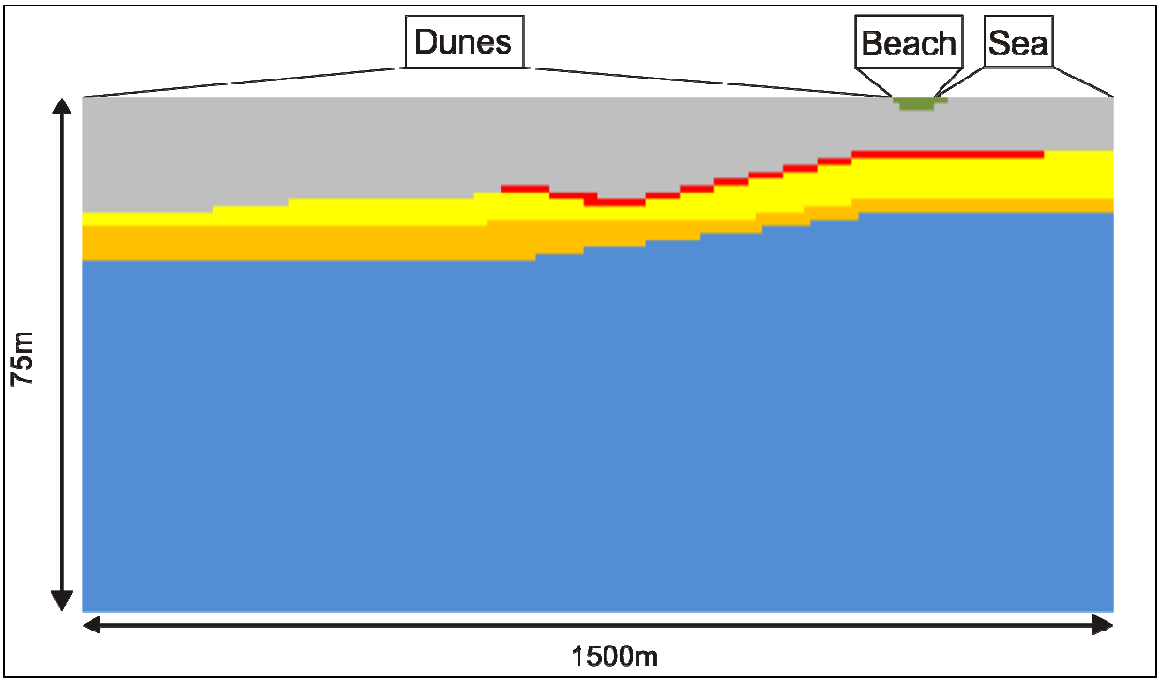

Figure 4.4 *Configuration of hydrogeological units applied in simulation 2. The 'Loam' unit extends to 200m from the beach.*

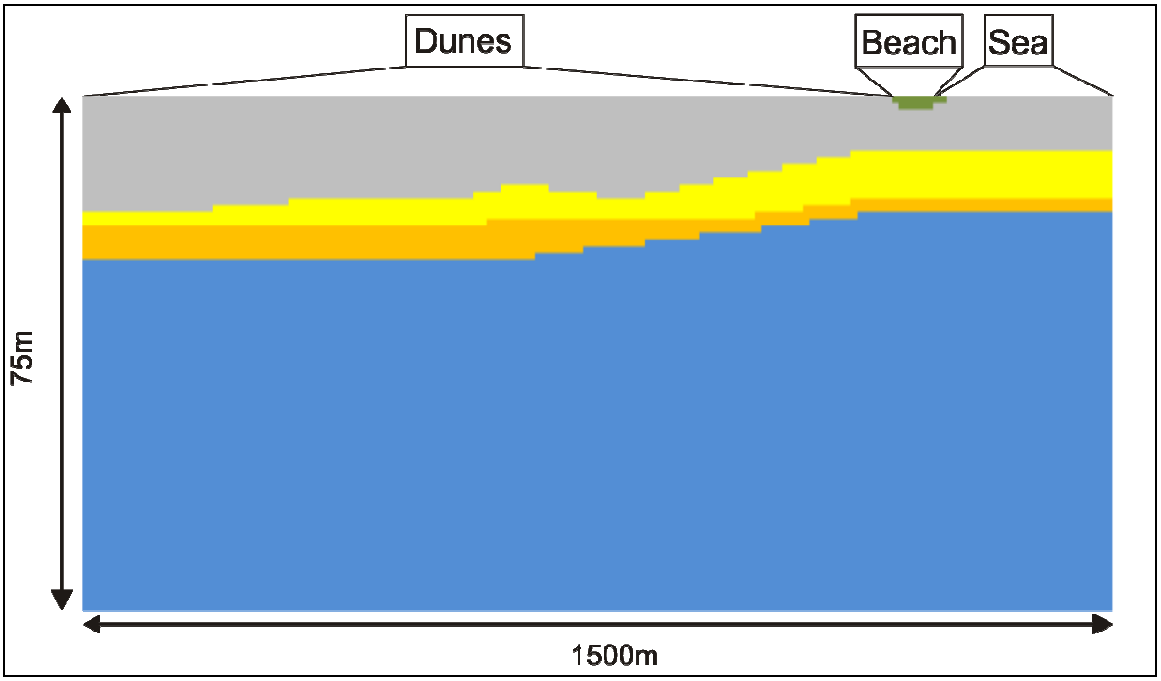

Figure 4.5 *Configuration of hydrogeological units applied in simulation 3. The 'Loam' unit is neglected in this simulation.*

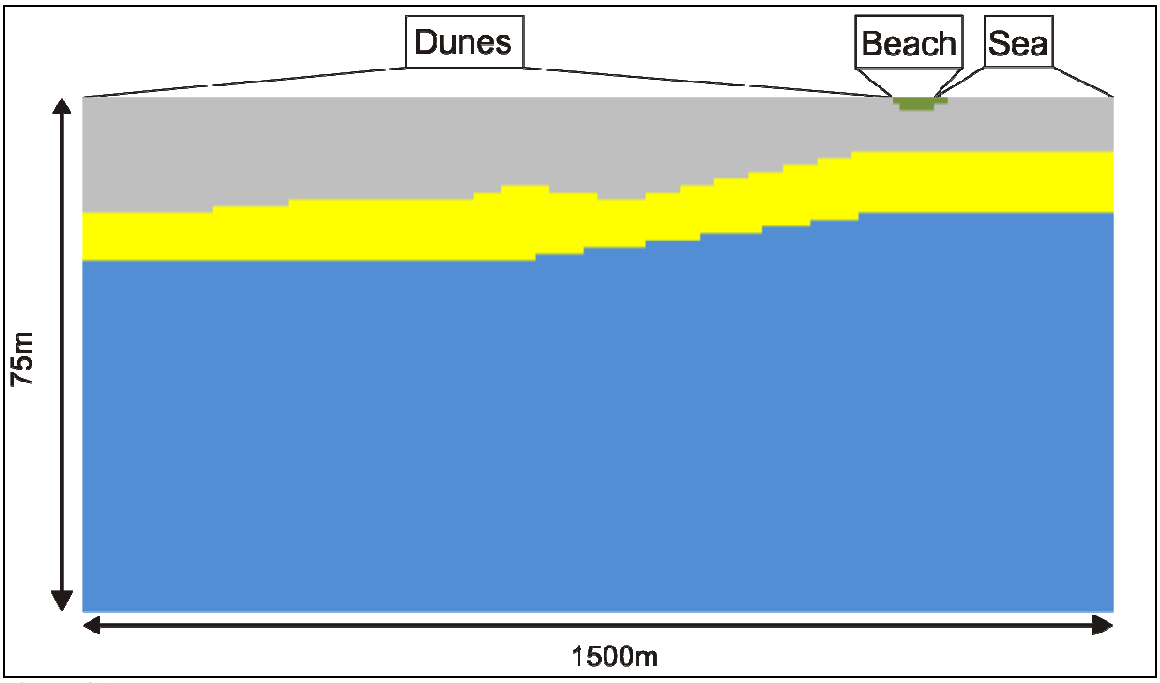

Figure 4.6 *Configuration of hydrogeological units applied in simulation 4. The 'Loam' and the 'Till & Clay' units are not incorporated in this model simulation.*

4.3 Results

Results of the four simulations after 100, 300, 500 and 1000 years are shown in figures 4.7, 4.10 – 4.12. The x axis is positive in the direction of the sea. The z axis is negative downward. In the following description of the results, several terms and locations are used. The 'deep fresh-salt groundwater interface' refers to the interface from fresh to salt groundwater in the downward direction between -30m and -100m. With 'shallow salt-fresh groundwater interface' the interface is meant which is present between 0 and -30m. With 'beach', cells 121-125 are meant, so the low water line is located at x = 1260m. Last, infiltration at the beach refers to the specified flow in cells 121-125.
The computed hydraulic heads are not shown in the figures. In all numerical model simulations, hydraulic heads in the dunes were comparable with the field observations. Near the beach however, the computed hydraulic heads were almost twice as a high as was observed. This implied an overestimation of the amount of seawater that infiltrates, or an underestimation of the hydraulic conductivity of the subsurface. The amount of seawater infiltration was first halved. The effect on the hydraulic head at the beach was however minor. In simulation 3, where the 'Loam' unit is not incorporated, hydraulic heads at the beach are also too high suggesting that this unit has little effect on the hydraulic heads at the beach. The hydraulic conductivity of the 'Holocene' and 'Pleistocene' units was therefore changed until proper hydraulic heads were obtained. A modification of the 'Pleistocene' unit from 4 m/d to 5 m/d was enough to sufficiently decrease the hydraulic head at the beach. The salinity distribution was however not significantly modified by this, so no results of this simulation are shown.

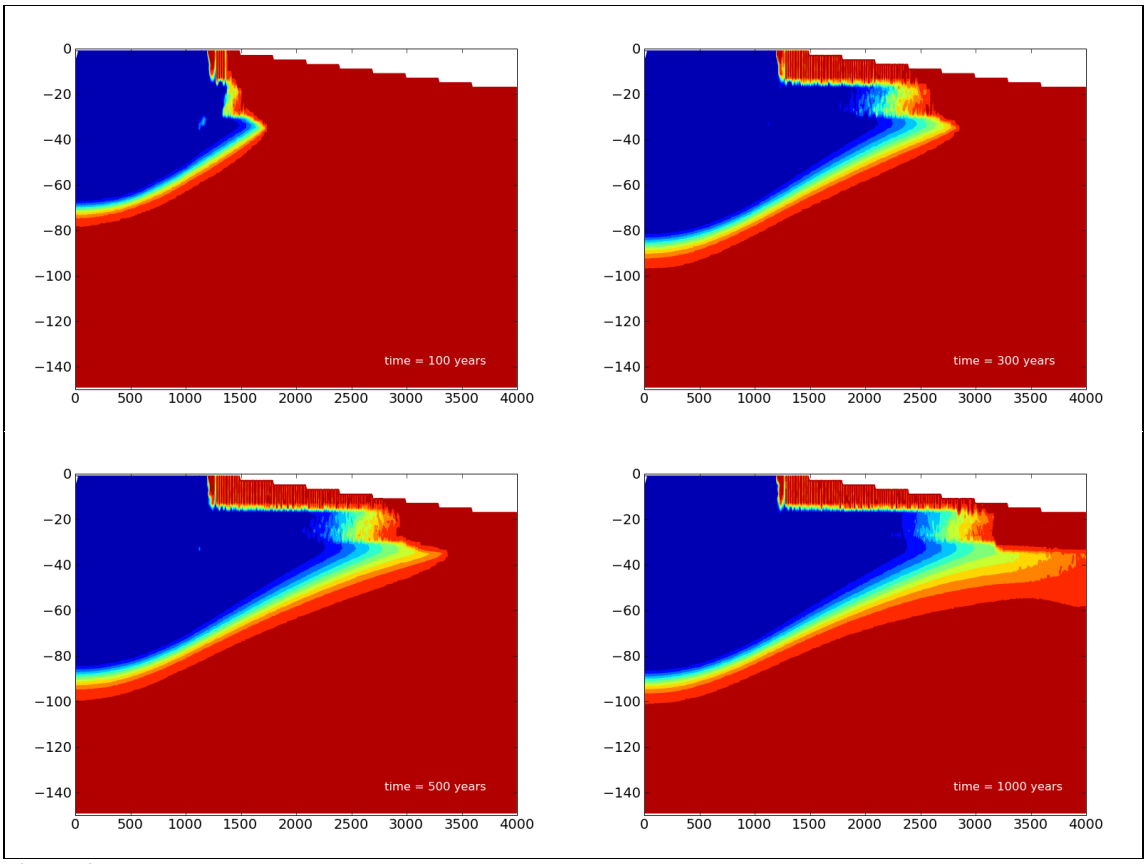

Figure 4.7 *Results of simulation 1, where the 'Loam' and 'Till & Clay' units have been incorporated.*

Figure 4.7 depicts the results of simulation 1. After 500 years, the depth of deep fresh salt interface for the onshore part of the model is stable. At the groundwater divide, the interface is located at approximately 90m –MSL, while at the beach the interface is at 70m –MSL. After 1000 years, the tongue is still extending offshore. Although the dispersivity is set to a relatively low value, a significant mixing zone is observed at the front and the bottom of the developing fresh submarine groundwater tongue underneath the 'Clay & Till' unit. Because flow rates decrease downward below this unit, freshening is slower at the bottom of the fresh submarine groundwater tongue. This results in a curved shape (Figure 4.8) of the developing freshwater tongue.

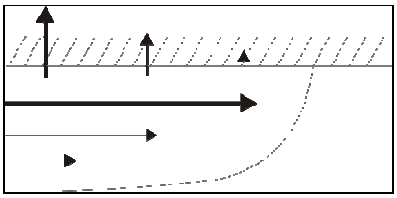

Figure 4.8 *Sketch of the curved shape of the developing fresh submarine groundwater tongue below a resistant layer. The difference in length and thickness of the arrows indicate the relative difference in flow rates.*

Freshening below the 'Loam' unit is slower than below the 'Clay & Till' unit because of the upward seepage across the 'Loam' unit. Above the 'Loam' unit, upward seepage of fresh groundwater and downward density driven flow of salt groundwater, result in a complex mixing zone. This is probably not correctly modeled because of the coarse grid spacing.
A small zone of brackish groundwater flowing upward and discharging across the seabed is present just seaward of the low water line. The shallow groundwater salinity distribution below the beach is not stable over time. Again, this is probably caused by the too large grid spacing. Near the low water line, the depth of the salt-fresh groundwater interface is modeled at -16m,

which is comparable with the field observations. The depth of the interface is caused by the presence of the 'Loam' unit from 16 – 18m –MSL, which prevents further downward movement of the infiltrated seawater. The salinity distribution toward the high water line is not comparable with the field observations because the depth of the interface is simulated deeper than was observed. An extra simulation was therefore performed, where less seawater infiltrates at the beach. Here it was assumed that the beach was not able to drain till field capacity during low tide, but instead a pF of 1.5 was assumed, corresponding to a volumetric water content of 0.2. The resulting input values for cells 121-125 can be found in Table 4.5. The results are shown in figure 4.9.

Table 4.5 *Cell input values applied in simulation 5*

Dunes						**Sea**
Model cell nr.	121	122	123	124	125	
Recharge in $m^3\ m^{-2}\ yr^{-1}$	63	156	250	125	0	

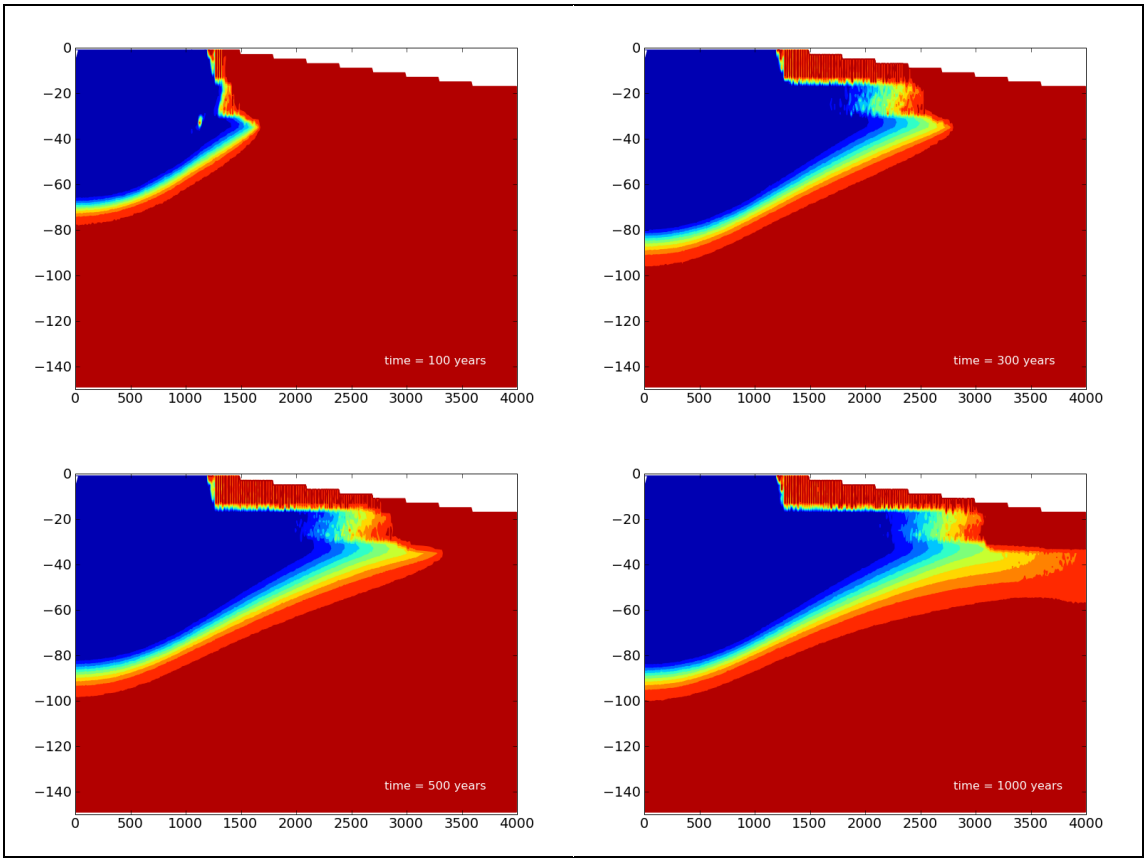

Figure 4.9 *Results of a simulation where the configuration of hydrogeological units of simulation 1 is applied, but a different amount of seawater infiltration at the beach (Table 4.5).*

Figure 4.9 shows that by reducing the amount of infiltrating seawater, the salt-fresh interface below the beach is also reduced. This is most pronounced at the high water line. In this way, a reasonable match with the field measurements is obtained. However, the distribution is unstable throughout the simulation. This is again believed to be the result of the large grid spacing.

Figure 4.10 depicts the model results of simulation 2. The deep groundwater salinity distribution and the development of the fresh submarine groundwater tongue is comparable with simulation 1. The more shallow distribution of salt and fresh groundwater clearly indicates the absence of the 'Loam' unit from x = 1500m. A small zone of near-vertical flowing brackish groundwater is observed at the end of the 'Loam' unit, which ultimately

discharges across the seabed. Like in simulation 1, submarine groundwater discharge takes place just seaward of the low water line.

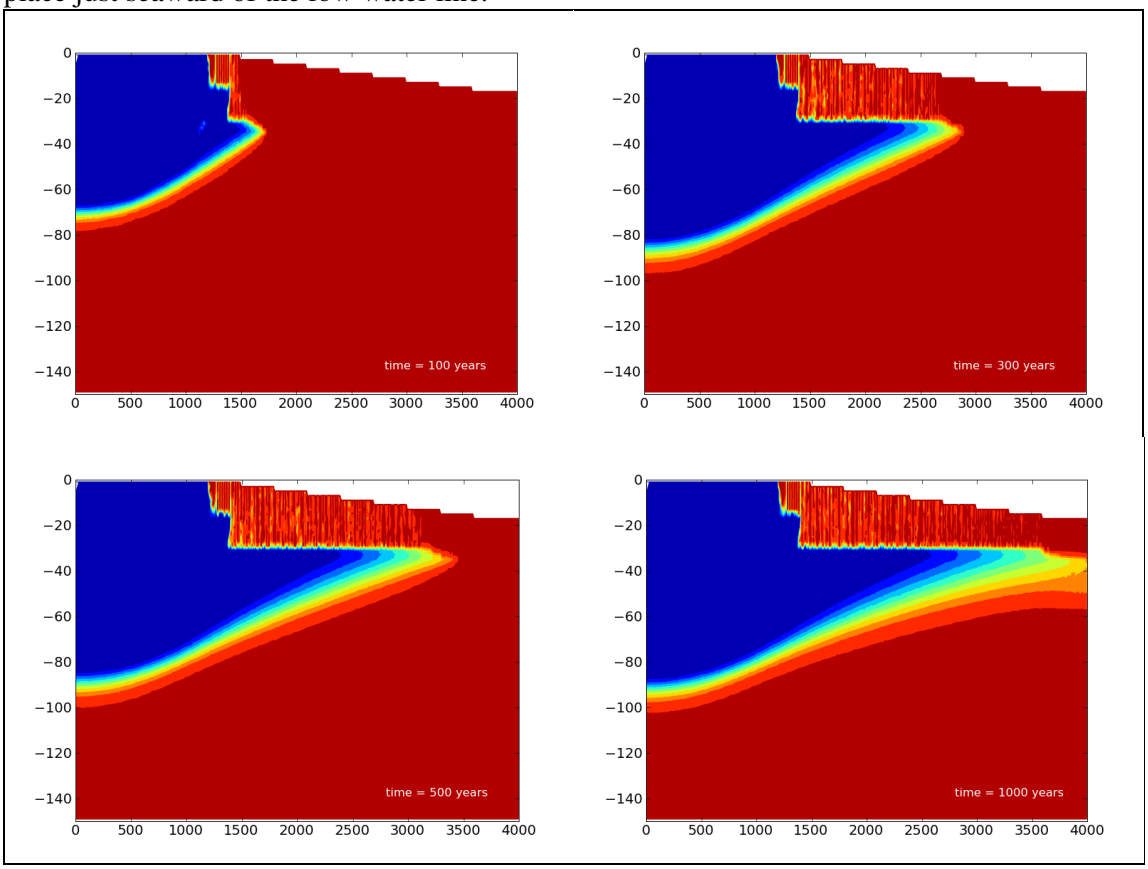

Figure 4.10 *Results of simulation 2, where the 'Loam' unit extends 200m from the beach.*

In figure 4.11, the results of simulation 3 are shown where the 'Loam' unit is not present. The deep groundwater salinity distribution is barely affected by the absence of this unit and thus comparable with simulations 1 and 2. The shallow groundwater salinity distribution is however different. The salt-fresh groundwater interface at the low water line is deeper (± -25m) because the downward flowing seawater which infiltrated at the beach is not affected by this unit. The submarine groundwater discharge zone is somewhat wider and less saline.
The results of simulation 4, where both resistant units are absent, are shown in figure 4.12. The groundwater salinity distribution clearly deviates from the previous simulations. A submarine fresh groundwater tongue is not observed. The deep fresh-salt groundwater interface is located at -90m on the left side of the model and decreases more in the seaward direction than in simulations 1-3. At the low water line, no deep fresh groundwater is present. The shallow salt-fresh groundwater interface is unstable. This is caused by the downward, relatively fast flowing seawater that infiltrates at the beach and the coarse grid spacing. The zone where submarine groundwater takes place is therefore also not stable throughout this simulation, although it seems that this zone is more pronounced and less saline compared to simulations 1 and 2.
As expected, the computed hydraulic heads are too low because the 'Clay & Till' layer is not present.

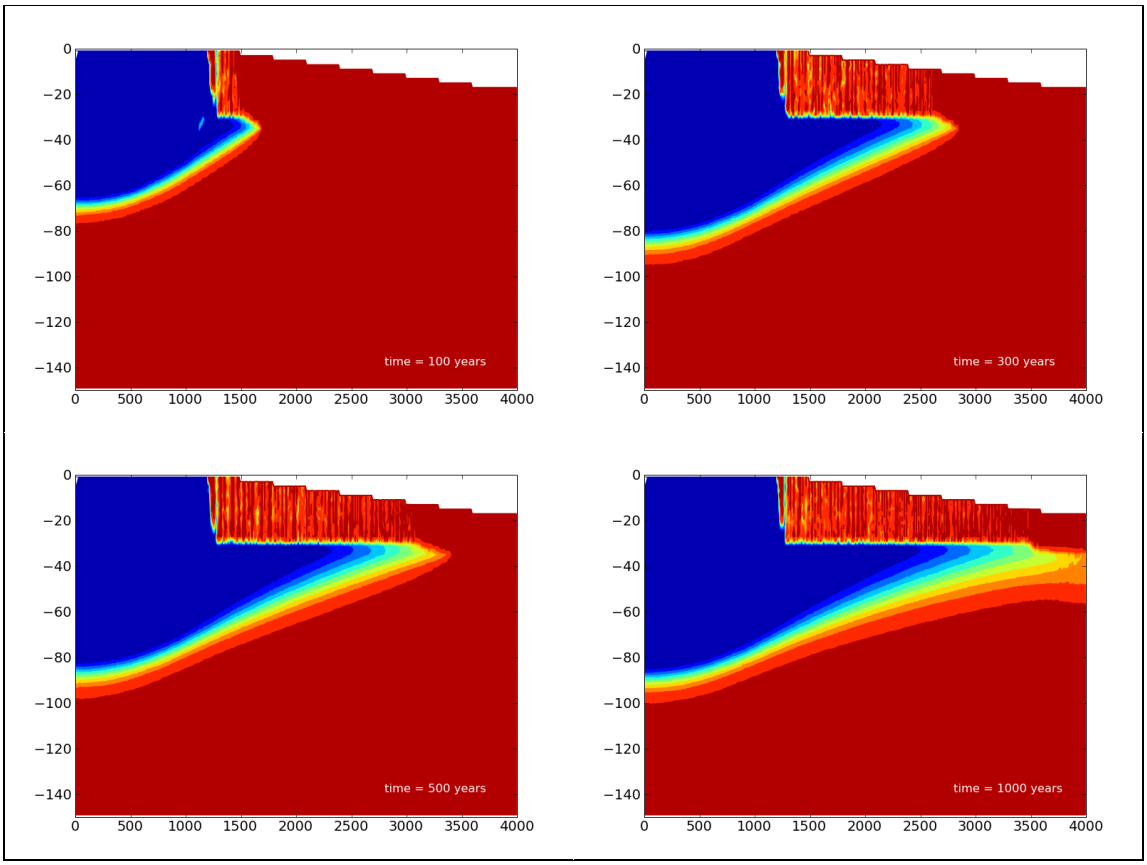

Figure 4.11 *Results from simulation 3, where the 'Loam' unit has not been incorporated.*

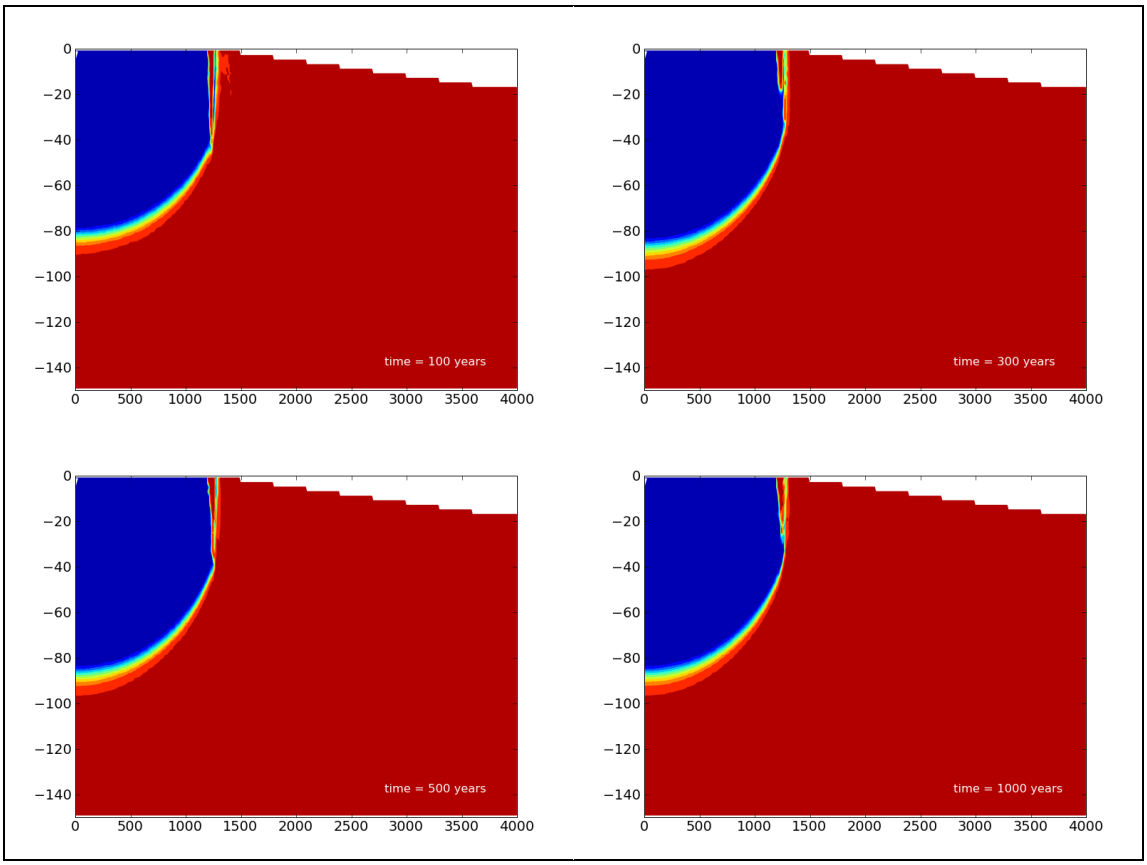

Figure 4.12 *Results of simulation 4, where no resistant units are present.*

5 Discussion

5.1 Alongshore variations in groundwater salinity at the beach

CVES measurement 4 indicates minimal alongshore variations of the groundwater salinity in the vicinity (<200m) of the research transect. The FDEM transects (1,2 and 3) near the research transect did also not show significant alongshore variations of the groundwater salinity. Significant higher conductivities were however measured by FDEM survey at 2km south of research transect, indicating more saline groundwater conditions here.
An alongshore FDEM survey by Biewinga et al. (1991), yielded comparable outcomes, where the conductivity around beachpost 4400 was significantly higher than around beachpost 4200. The same instrument and the horizontal dipole configuration with a coil distance of 20m were used in this study. Although measurements were taken between the high water line and the dunefoot, the exact position from the dunefoot has not been described in detail. The FDEM survey showed that the conductivity of the beach subsurface strongly depends on the position from the dunefoot. Nevertheless, the conductivity results were related to alongshore variations in geology, using nearby borehole data as validation data. The measurement results and interpretation can be found in Appendix E. The geological interpretation reveals a higher clay content in the upper 20m of the beach subsurface around beachpost 4400. This could be an explanation for the measured conductivity of the subsurface, but cannot be concluded with certainty.

5.2 Groundwater salinity variations at the beach over a spring-neap tidal cycle

The CTD diver measurements showed that the groundwater salinity near the low water line and in between the low and the high water line is relatively stable in time, compared to the high water line. At the high water line, mixing of fresh groundwater flow from the dune area and infiltrated seawater occurs. Over time, this results in a dynamic salinity of the groundwater. A fluctuating salinity of the groundwater near the high water line, measured at a comparable depth from the beach surface, was also observed by Robinson et al. (2007b). Robinson et al. further observed strong temporal salinity changes near the low water line, indicating submarine groundwater discharge here, and to a lesser extent in between the low and high water line. Significant salinity changes were however not observed at comparable locations at the research transect. Although the water level variations were comparable, the measured beach slope by Robinson et al. was higher. As a result, the intertidal zone is smaller (around 30m). This explains the higher and more stable salinities at the research transect as more salt water is able to infiltrate here. Numerical simulations by Robinson et al. (2007a) verify this by showing that the upper salt water wedge on the beach increases as the extension of the intertidal zone (by increasing the amplitude of the tidal boundary condition) is increased. The discussion on the possible presence of a zone of brackish submarine groundwater discharge is given in section 5.3.
Temperature observations indicate that upward flow near the low water line takes place during low sea level, while a high sea level favors downward flow here. Furthermore, the EC of the groundwater at the low water line slightly dropped in a period of relatively low sea levels (Figure 3.24), indicating the upward transfer of less saline groundwater.

5.3 Measurements and modeling results along the research transect

Figure 5.1 depicts an overview of the groundwater salinity along a part of the research transect, based on the results of the field measurements. The geophysical measurements indicated that the deep fresh-salt groundwater interface decreases from the groundwater divide (90m –MSL) to the beach (70m –MSL). The shore normal CVES measurement indicated the presence of a salt water wedge, where the salt-brackish groundwater interface increases in depth from the storm high tide mark toward the sea. The brackish-fresh groundwater interface also increases in depth from the dunes toward the sea. These interfaces are drawn in figure 5.1, but are thought to vary in time due to the dynamic hydrological boundary conditions (e.g., precipitation, fresh groundwater flow from the dunes, sea level).
A comparable configuration of the base of the freshwater lens has been computed in numerical simulations 1, 2 and 3, from 90m –MSL at the groundwater divide to -70m at the beach. Simulation 4 was able to compute a comparable interface depth at the groundwater divide, but yielded a shallower interface at the beach. These observations indicate that the low permeable sediments of the Eem formation, simulated by the 'Till and Clay' unit, are of influence on the deep fresh-salt groundwater interface at the beach of the research location. It must be noted here that only the current hydrological boundary conditions have been considered. A short discussion on former hydrological settings and their influence on the deep fresh-salt groundwater interface is given at the end of this paragraph.
All numerical models showed an instable salinity distribution for the zone beneath (<30m - MSL) the beach. This is thought to result from the too large grid spacing. A reduced amount of seawater infiltration had to be applied (adapted simulation 1) to obtain a comparable groundwater salinity distribution with the field measurements, for the upper 20m below the average intertidal zone. Simulations 3 and 4 did not yield a comparable groundwater salinity distribution for the zone beneath the beach. Furthermore, these simulations indicated a wider and less saline submarine groundwater zone. The resistant layers therefore influence the shallow (<30m –MSL) groundwater salinity distribution, and reduce the upward flow of fresh groundwater toward the low water line.
Shallow brackish groundwater near the low water line, revealing a submarine groundwater discharge zone, was not indicated by the field measurements. No measurements were however performed seaward of the low water line, so this zone is possibly located here (Figure 5.2). Another explanation is that the upward flow of fresh groundwater near the low water line is too small to form a distinct zone of brackish submarine discharge (Figure 5.3).
Storms result in occasional seawater infiltration near the dune foot. This was indicated by the shore normal CVES measurement 1, but this was not simulated in the model. A slight modification of the hydraulic conductivity of the 'Pleistocene' unit was needed to obtain similar hydraulic heads at the beach as measured in the field.
When low permeable sediments continue offshore, a fresh submarine groundwater tongue develops. The offshore extension of the low permeable units therefore determines the extension of the freshwater tongue, as is shown in simulation 2.
The observed distribution of salt and fresh groundwater can thus be explained by the current hydrological boundary conditions. As was already mentioned, annual rainfall, sea level, land and sea bottom elevation and the position of the shoreline have changed over the pas centuries, while these processes have not been simulated by the model. The observed deep fresh-salt groundwater interface at the beach could have been the result of a changing coastline. At approximately the start of the Middle Ages (500 AD), the coastline of the Netherlands was situated several hundred meters from the current coastline (Berendsen, 1998). In the area in between, fresh groundwater recharge from precipitation formed freshwater lenses. The measured base of current freshwater lens (Figure 3.25) could therefore have been the result of these former freshwater lenses. This is shown in figure 5.4. The question remains if the

infiltrating seawater by a retreating coastline was able to salinize the freshwater lens. Sedimentation and erosion and the elevation changes of the land and sea bottom also can have a significant impact on the offshore and onshore groundwater flow. Changes in annual rainfall are thought to have played a relatively minor role.

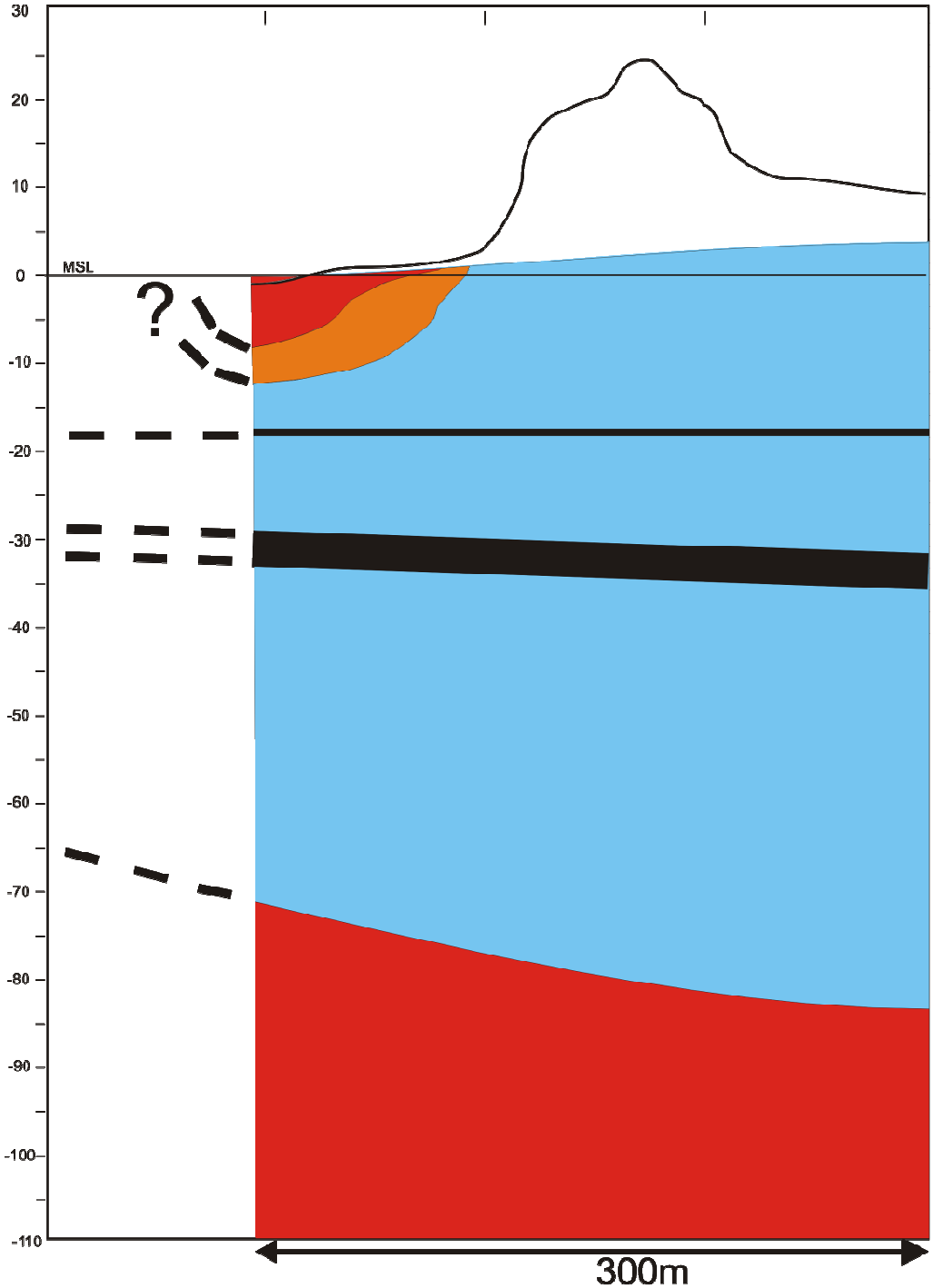

Figure 5.1 *Overview of groundwater salinity distribution along a part of the research transect, based on the results of the field measurements. The thick black lines indicate resistant layers in the subsurface. Numbers on the left are the depth/altitude in m relative to mean sea level. No offshore measurements were performed. Different scenarios for the shallow groundwater salinity distribution are given in figures 5.2 and 5.3.*

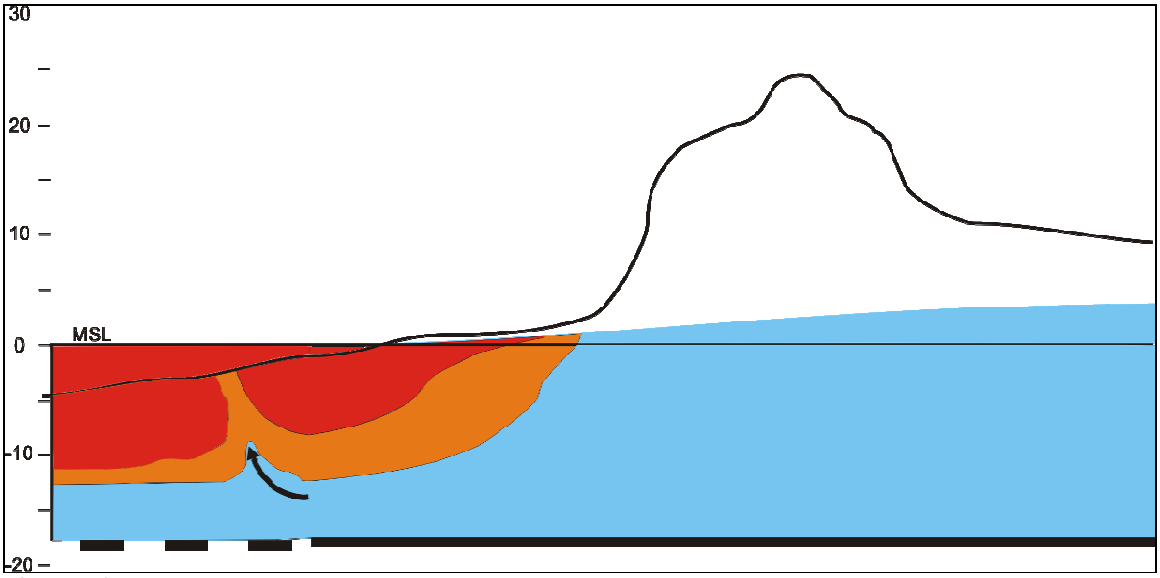

Figure 5.2 *Sketch of the shallow groundwater salinity distribution along the research transect, if a zone of brackish submarine groundwater discharge is present seaward of the low water line.*

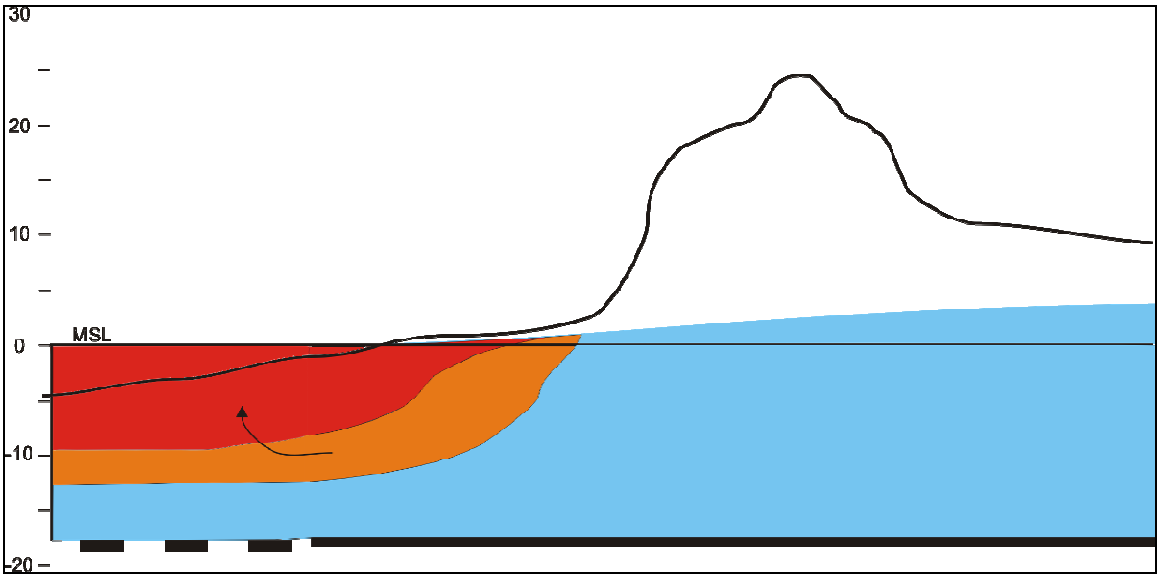

Figure 5.3 *Sketch of the shallow groundwater salinity distribution along the research transect, if the upward flow of fresh groundwater to the seabed in too small to form a brackish submarine groundwater discharge zone. Note that submarine groundwater discharge can still be present.*

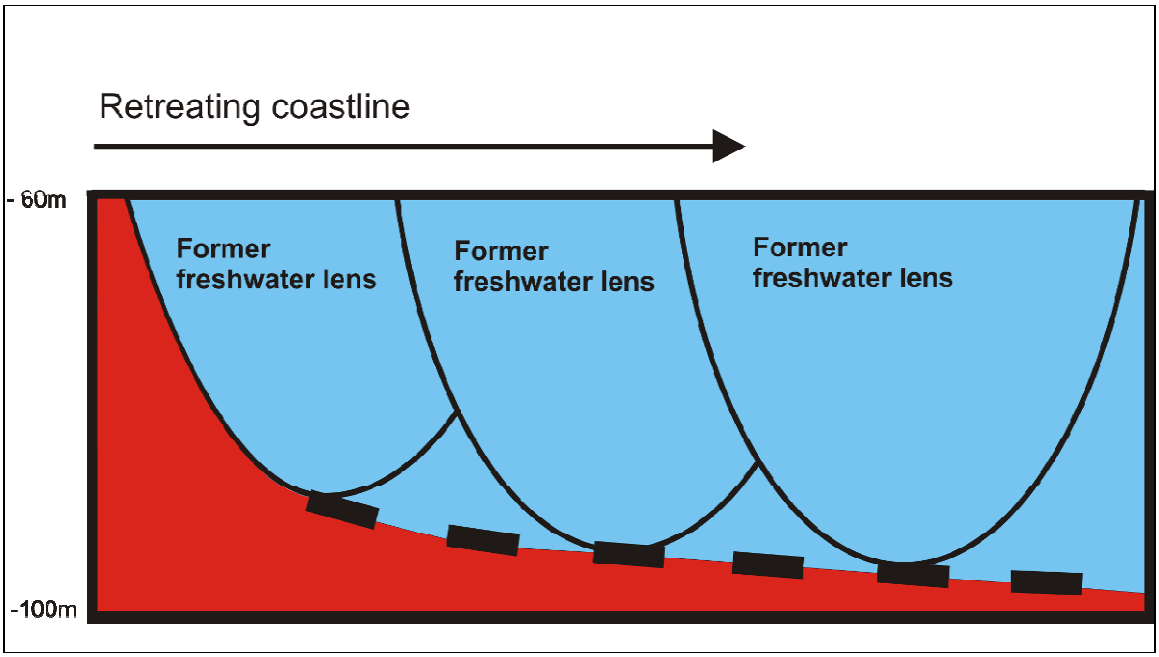

Figure 5.4 *Simplified sketch of a retreating coastline and location of former freshwater lenses, which could explain the deep fresh-salt groundwater interface that was measured at the beach (-70m). The numbers on the left indicate the depth relative to the current mean sea level. The increasing depth of the base of the freshwater lens with a retreating coastline is based on the assumption that the former dunes were lower than the current dunes.*

5.4 Comparison with other studies

The measured and simulated 'inverse' groundwater salinity distribution at the beach has also been indicated by Vandenbohede and Lebbe (2006) and Robinson et al. (2007a, 2007b), in numerical simulations and field measurements. Vandenbohede and Lebbe (2006) simulated fresh groundwater flow from the hinterland toward the sea and seawater infiltration at the beach in a homogenous, phreatic aquifer extending 30m from the mean sea level. This density distribution is unstable under hydrostatic conditions. Vandenbohede and Lebbe (2006) found out that the fresh-salt groundwater interface is relatively stable in time because the groundwater is in 'dynamic equilibrium'; the downward moving salt groundwater is mixed with the seaward flowing fresh groundwater toward the submarine groundwater discharge zone. Their model indicates that this submarine groundwater zone of low salinity is relatively wide (±80m) and located just seaward of the low water line. Robinson et al. (2007a) found similar groundwater salinity distributions on the beach with numerical model simulations, although the dimensions of the salt water wedge and the width of the submarine groundwater discharge zone were less than the results of Vandenbohede and Lebbe (2006). This is the result of the difference in hydrological boundary conditions, especially the width of the intertidal zone and therefore the amount of seawater infiltration here.
An important boundary condition in the numerical simulations of Vandenbohede and Lebbe (2006) and Robinson et al. (2007a, 2007b) is a no flow boundary at 30m –MSL. This boundary forces the fresh groundwater to discharge across the seabed, as opposed to the numerical simulations in this study, where fresh groundwater can also form a submarine groundwater tongue. Consequently, the upward freshwater flow toward the low water line is less. It is therefore expected that if a zone of submarine groundwater discharge along the research transect is present (Figure 5.2), it is less saline and less wide than was observed and computed in the above described studies. Robinson et al. (2007a) showed that as the freshwater flow from

the hinterland decreased, the upper salt water wedge expands while the submarine groundwater discharge zone narrows.
The offshore limit of the fresh groundwater tongue when low permeable units continue offshore, has not been investigated in this study. Numerical simulations by Groen (2002) showed that when a low permeable unit extends far enough offshore, the offshore limit of the freshwater tongue is where the upward seepage from the aquifer becomes so small that downward diffusive salt transport reaches into the aquifer and creates instability and convective density currents.

6 Conclusions and recommendations

Considering the objectives of this study, the following can be stated:

Mapping and simulating the distribution of fresh and saline groundwater in a cross section perpendicular to the coast.
The phreatic level is around 5m MSL near the groundwater divide and has a seasonal fluctuation (± 0.7m). In the centre of the dunes, the hydraulic gradient is around 0.003. Close to the sea it increases to 0.007.
The depth of the deep fresh-salt groundwater interface is around 90m –MSL at the groundwater divide and -70m –MSL at the beach. Salt and brackish groundwater is found on top of fresh groundwater at the beach, where the salt-brackish groundwater interface increases in depth from the storm high tide mark (2m) toward the sea (7m).

Investigate to what extent the current hydrological boundary conditions can explain the observed onshore groundwater salinity distribution.
The present boundary conditions at the research transect can explain the observed groundwater salinity distribution from the groundwater divide to the beach. Resistant units influence this groundwater salinity distribution. The downward flow of infiltrating seawater in the intertidal zone, is hindered by a relatively thin (<15cm) loam layer at -18m MSL. Numerical simulations showed that the upward flow of fresh groundwater toward and across the seabed (submarine groundwater discharge) close to the low water line is also hindered by this layer. A thicker (4m) resistant unit from -30 to -34m MSL also reduces the upward flow of fresh groundwater. This upward flow is higher when resistant layers are absent. When impermeable layers are present in the subsurface, fresh groundwater flow toward the submarine groundwater discharge zone is presumably even higher, as was deduced from other studies (Vandenbohede and Lebbe, 2006, Robinson 2007a, 2007b). A submarine groundwater discharge zone of significantly lower salinity has not been indicated by the field measurements in this study.
When the resistant units continue offshore, a submarine fresh groundwater tongue is formed.

Giving insight into the dynamics of groundwater level, salinity and temperature at the beach, over a spring-neap tidal cycle.
The groundwater level at the beach is driven by the sea level. The sea level varies by the tide, but also depends on wind conditions.
The largest salinity changes in the intertidal zone were observed near the high water line, where fresh groundwater from the dune area mixes with infiltrated seawater. Near the low water line and in the middle of the intertidal zone, the groundwater salinity is relatively stable in time.
The temperature of the groundwater in the middle of the intertidal zone and near the high water line reflects the temperature of the seawater, so seawater infiltration takes place here. No tidal influence was found here. At the low water line, the groundwater temperature deviates from seawater and indicates former infiltrated seawater. Seawater infiltration is less than at the higher part of the intertidal zone. A tidal influence is found here when the wind is calm and the seawater level is relatively low. In these calm periods, upward flow takes place during low sea level, and little seawater infiltrates during high sea level.

From the results of this study, the following is recommended:

Because a submarine groundwater discharge zone of lower salinity has not been indicated by field measurements along the research transect, field measurements seaward of the low water line have to be performed to investigate whether this zone is present or not. A cross shore marine CVES measurement (80m profile length, ±12m exploration depth) can indicate this. To model groundwater flow on the scale of the beach, a small grid size is necessary. This increases however the computational efforts considerably. Special attention should be given on the extent of the model and the hydrogeological configuration. Furthermore, the effects of wind and storms on sealevel have to be incorporated when a tidal boundary condition is applied.

7 Acknowledgements

I very appreciate the help of my three supervisors. Koos Groen, thank you for initiating and organizing this project. Michel Groen, thank you for your support and guidance in all the field activities, for your research ideas and our productive discussions on the field measurements. Vincent Post, thank you for your help with the numerical model and the construction of the Python script. Thank you all for reading and correcting my report.
Thanks to Frans Backer, who was involved in nearly all fieldwork activities. It was nice to work with Jelle Jan Pieterse in the field and the laboratory.
For the hydrological and geological data and the permission to perform field measurements in the dune area, I would like to thank Harry Rolf and Sander de Haas of the Provincial Water supply company of North Holland (PWN). Thanks to Jouke Velstra of Acacia Water who provided useful data for the numerical model experiments. Thanks to Royal BAM and WINN for funding several field measurements. For the GIS TOP10 vector 2003 topographical data, I would like Alfred Wagtendonk of the Institute for Environmental Studies at the VU University Amsterdam.

8 Bibliography

ABEM, 1994. *Instruction Manual Terrameter SAS 300 C*. Printed matter No 93060. ABEM Instrument AB, Allén 1, S-172 66 Sundbyberg, Sweden

ABEM, 2009. *Instruction Manual SAS 4000 / SAS 1000*. Printed matter No 93109. ABEM Instrument AB, Allén 1, S-172 66 Sundbyberg, Sweden

AHN, 2009. Online Actual Elevation Data of the Netherlands (Actueel Hoogtebestand Nederland). Website: www.ahn.nl

Biewinga, D.T., Pruissers, A.P. and Seijmonsbergen, A.C., 1991. *De geologie van het kustprofiel tussen Wijk aan Zee en de Hondsbossche Zeewering en een geofysiche verkenning*. H_2O (24) 1990, p692-697. (In Dutch)

Geotomo, 2004. *RES2DINV ver. 3.54 for Windows 98/Me/2000/NT/XP*. Geotomo Software, 5 Cangkat Minden Lorong 6, Minden Heights, 11700 Gelugor, Penang, MALAYSIA

Berendsen, H.J.A., 1998. *De vorming van het land. Inleiding in de geologie en geomorfologie.* Van Gorcum & Comp. B.V., Assen, p. 70-170 (In Dutch).

Bakker, T.W.M., 1981. *Nederlandse kustduinen: geohydrologie*. Ph.D. Thesis, PUDOC Wageningen, 189p. (In Dutch)

Breukelen, B.M. van, Groen, M.M.A., Groen, J., Huissteden, J. van, de Jeu, R.A.M., Post, V.E.A., Schellekens, J., Smit, P., and Waterloo, M.J. *Handbook for Field Hydrological Measurements*. Faculty of Earth and Life Sciences, Vrije Universiteit Amsterdam, 2007.

Caljouw, M., 2000. *Video-based monitoring of the Egmond beach- and shoreface nourishments*, Voortschrijdend Onderzoek Programma (VOP) WL Delft Hydraulics, Z2773 (in Dutch).

Chiang, W.H., 2005. *Processing Modflow Pro version 7.0.31*. Integrated Environmental Services, Inc. Lake Forest, California 92630, USA

Dinoloket, 2009. Data and Information of the Dutch subsurface. Toegepast Natuurwetenschappelijk Onderzoek -Nederlands Instituut voor Toegepaste Geowetenschappen (TNO-NITG). Website: www.dinoloket.nl

Domenico, P. A., Schwartz, F. W., 1990. *Physical and chemical hydrogeology*. John Wiley and Sons, New York, USA.

Ecobeach, 2006. Online information on the Ecobeach pilot, Royal BAM Group nv, Bunnik, The Netherlands, website: www.ecobeach.nl (in Dutch)

Ecoshore, 2006. Online information on Pressure Equalizing Modules, Ecoshore International Inc, 2255 Glades Road, Suite 324A Boca Raton, FL 33431 USA, website: www.ecoshore.com

Groen, J., 2002. *The Effects of Transgressions and Regressions on Coastal and Offshore Groundwater*. Ph.D. Thesis, Vrije Universiteit, Amsterdam.

Guo, W., Langevin, C.D., 2002. *User's guide to SEAWAT: A computer program for simulation of three-dimensional variable-density ground-water flow.* U.S. Geological Survey Techniques of Water-Resources Investigations, book 6, chap. A7, 77 pp.

Harbaugh, A.W., Banta, E.R., Hill, M.C., and McDonald, M.G., 2000. *MODFLOW-2000, the U.S. Geological Survey modular ground-water model -- User guide to modularization concepts and the Ground-Water Flow Process*: U.S. Geological Survey Open-File Report 00-92, 121 p.

Hemker, C.J., Post, V.E.A. *SCHLUMBG for Windows. Interpretation of Resistivity Soundings with Schlumberger and Wenner Configuration.* Beta Version 1.0.02. Copyright by C.J. Hemker, Elandsgracht 83, Amsterdam.

Horn, D.P., 2006. *Measurements and modelling of beach groundwater flow in the swash-zone: a review*, Continental Shelf Research 26 (2006) 622–652.

Janssen, G.M., 2008. *Strand, meer dan zand*. Inaugural Speech, Vrije Universiteit, Amsterdam (in Dutch).

Jakobsen, P., Brøgger, C., 2007. *Coastal protection based on Pressure Equalization Modules (PEM)*, International Coastal Symposium 2007, Gold Coast, Australia.

Kooi, H., Groen, J., 2001. *Offshore continuation of coastal groundwater systems; predictions using sharp-interface approximations and variable density flow modelling*. J. Hydrol., 246, p. 19-35.

KNMI, 2000. *Langjarige gemiddelden en extremen, tijdvak 1971 – 2000 Normalen KNMI-neerslagstation.* Online precipitation data from the Royal Dutch Meteorological Institute (KNMI). Website: http://www.knmi.nl/klimatologie/normalen1971-2000/neerslag.html

KNMI, 2009a. *Hourly weather data in the Netherlands, station 'de Bilt'*. Online weather data from the KNMI. Website: http://www.knmi.nl/klimatologie/uurgegevens/#no

KNMI, 2009b. *Hourly weather data in the Netherlands, station 'Wijk aan Zee'*. Online weather data from the KNMI. Website: http://www.knmi.nl/klimatologie/uurgegevens/#no

Kuiper, M.J., 2007. *Topography-driven freshening of offshore aquifer systems during glacial periods.* MSc. Thesis. Vrije Universiteit, Amsterdam.

Manheim F.T., Krantz D.E., Bratton J.F., 2004. *Studying ground water under Delmarva coastal bays using electrical resistivity*. Ground Water-Oceans Issue 42(7):1052–1068

McNeill, J.D., 1980. *Electromagnetic terrain conductivity measurement at low induction numbers.* Technical Note TN-6, Geonics Limited, Mississauga, Ontario, Canada.

Oude Essink, G.H.P., 1996. *Impact of sea level rise on groundwater flow regimes: a sensitivity analysis for the Netherlands*. Ph. D. Thesis, Delft University of Technology.

Pieterse, J.J., 2009. The *influence of an Ecobeach PEM on beach development***.** Master Thesis, TU Delft

Prieto, C., and G. Destouni, 2005. *Quantifying hydrological and tidal influences on groundwater discharges to coastal waters*, Water Resour. Res. 41.

PWN, 2006. *Eindverslag Natuurherstelproject Doornvlak*. Provinciaal Waterleidingbedrijf Noord Holland (In Dutch).

Python, 2009. Open source, online available programming language. Python Software Foundation. www.python.org

Rijkswaterstaat, 2009. *Sea water temperatures at IJmuiden buitenhaven 2009*, dataset from the Dutch Department of Public Works (Rijkswaterstaat).

Robinson, C., L. Li, and D. A. Barry, 2007a. *Effect of tidal forcing on a subterranean estuary*, Adv. Water Resour., 30, p851 – 865,

Robinson, C., B. Gibbes, H. Carey, and L. Li, 2007b. *Salt-freshwater dynamics in a subterranean estuary over a spring-neap tidal cycle,* J. Geophys. Res. 112.

Stuyfzand, P. J., 1993. *Hydrochemistry and hydrology of the coastal dune area of the western Netherlands*. Ph.D. Thesis, Vrije Universiteit, Amsterdam.

Vandenbohede, A. and Lebbe, L., 2006. *Occurrence of salt water above fresh water in dynamic equilibrium in a coastal groundwater flow system near De Panne, Belgium*. Hydrogeology Journal 14: 462–472

Weerts, H.J.T., Cleveringa, P., Ebbing, J.H.J., de Lange, F.D., Westerhoff, W.E., 2003. *De lithostratigrafische indeling van Nederland. Formaties uit het Tertiair en Kwartair.* Report Nr. 03-051-A. Nederlands Instituut voor Toegepaste Geowetenschappen TNO, Utrecht: 38 pp.

Wolters-Noordhoff, 1988. *Grote Provincie Atlas Noord Holland 1:25000*. Topografic maps of the province of North Holland, scale 1:25000 (p 64). Wolters-Noordhoff Atlasproducties bv, Groningen, The Netherlands.

Zagwijn, W.H. & C.J. van Staalduinen (red.), 1975, *Toelichting bij geologische overzichtskaarten van Nederland*. Rijks Geologische Dienst, Haarlem (In Dutch).

Zonge, 2000. *ZT-30 ZeroTEM Transmitter manual*. Zonge Engineering and Research Organization, Inc. 3322 East Fort Lowell Road, Tucson, AZ 85716 USA

Zheng, C., Wang, P.P., 1999. *MT3DMS: documentation and user's guide.* Contract Report SERDP-99-1, U.S. Army Eng, R&D Center, Vicksburg, MS, USA, 220 pp.

9 Appendices

Appendix A

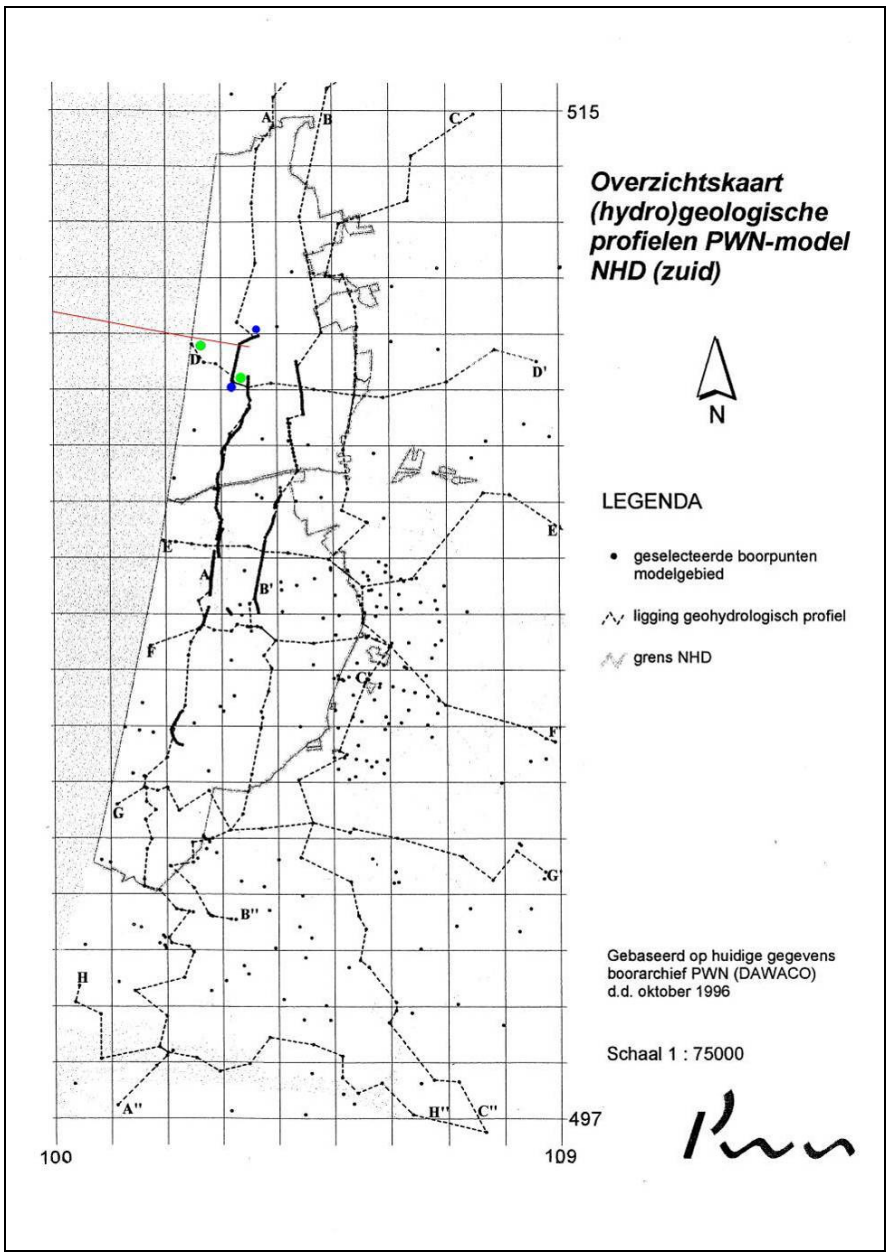

Appendix A: overview of the location of hydrogeological profiles from PWN (colored dots/Appendix B and C) and the research transect (red line, extended offshore).

Appendix B

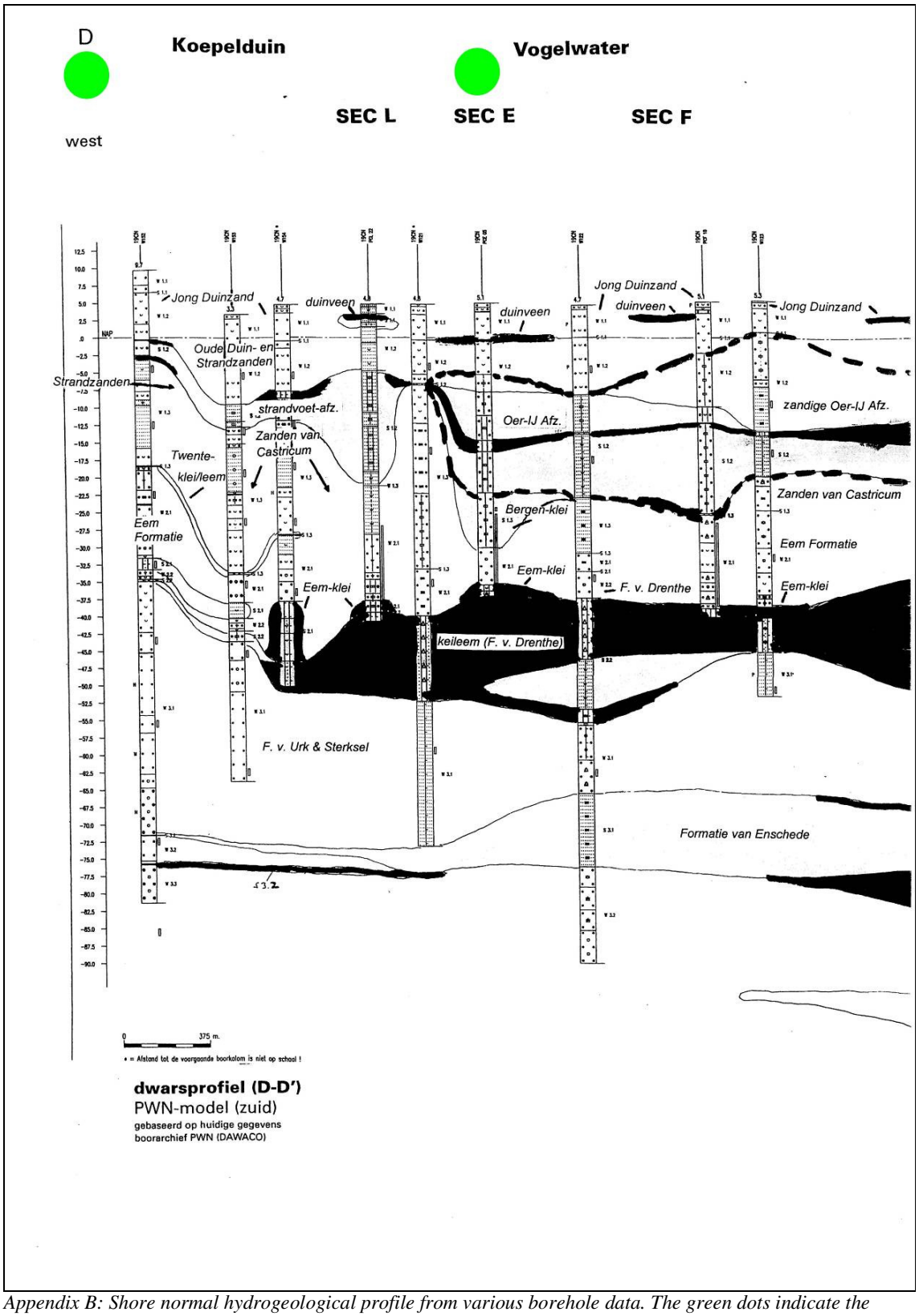

Appendix B: Shore normal hydrogeological profile from various borehole data. The green dots indicate the location shown in Appendix A. The formation names are based on the no longer used subdivision by Zagwijn en van Staalduinen (1975).

Appendix C

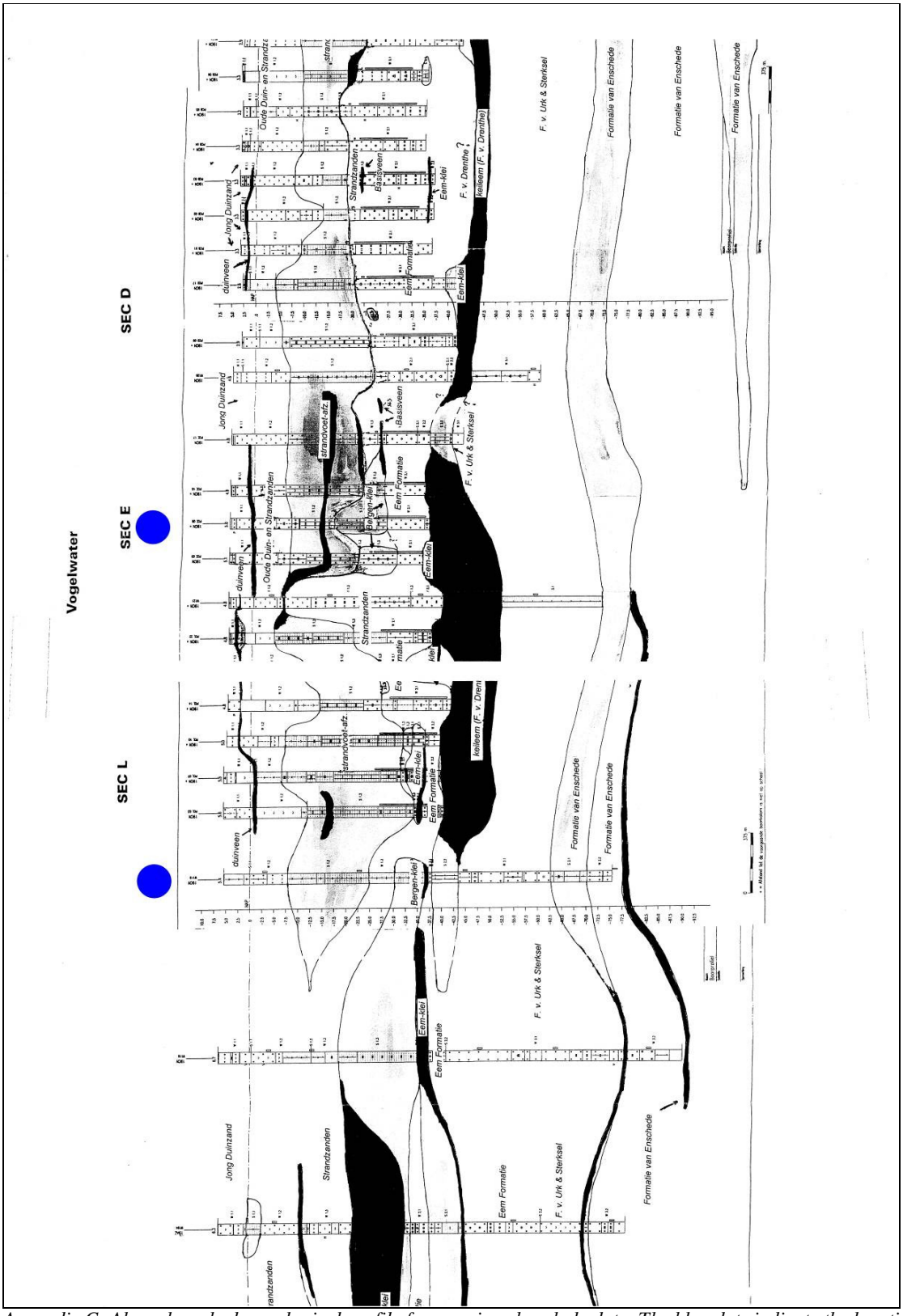

Appendix C: Alongshore hydrogeological profile from various borehole data. The blue dots indicate the location shown in Appendix A. Top is north, bottom is south. The formation names are based on the no longer used subdivision by Zagwijn en van Staalduinen (1975).

Appendix D

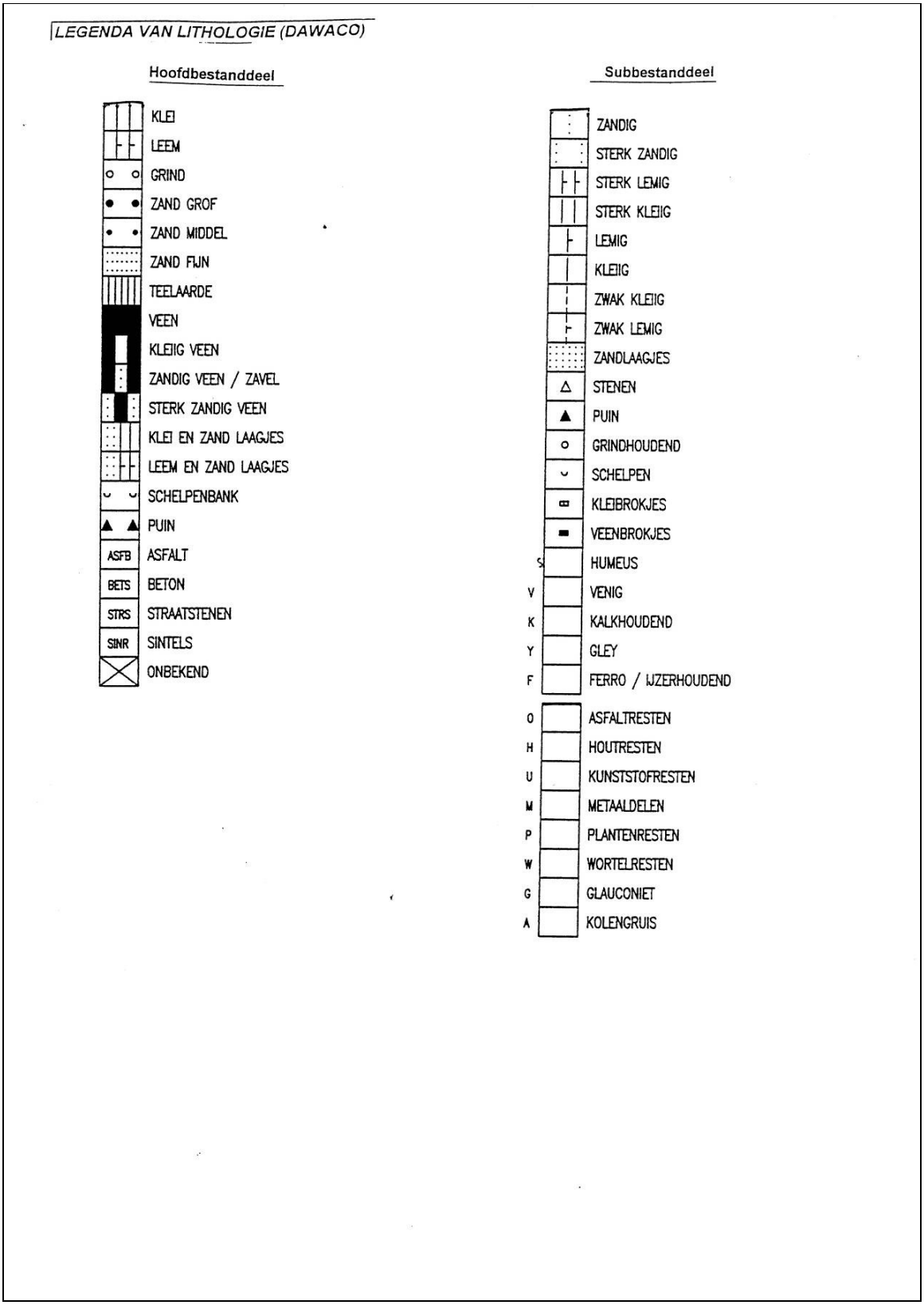

Appendix D: Legend of Appendices B and C (in Dutch).

Appendix E

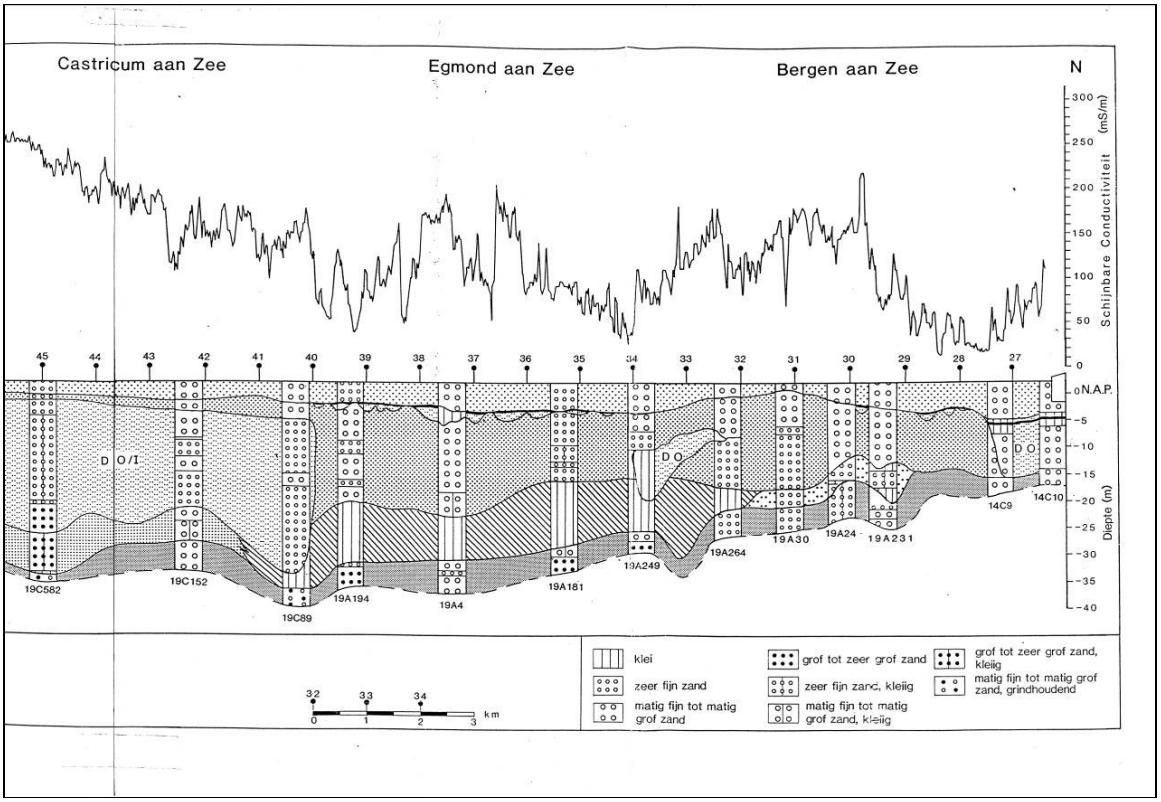

Appendix E: Apparent conductivity, borehole data and their interpretation of a transect along the beach (in: Biewinga et al. (1991)). The labels indicate cities shown in figure 1.1. Numbers just on top of the profile correspond to the beach post, where the research transect is located at '42'.

Appendix F

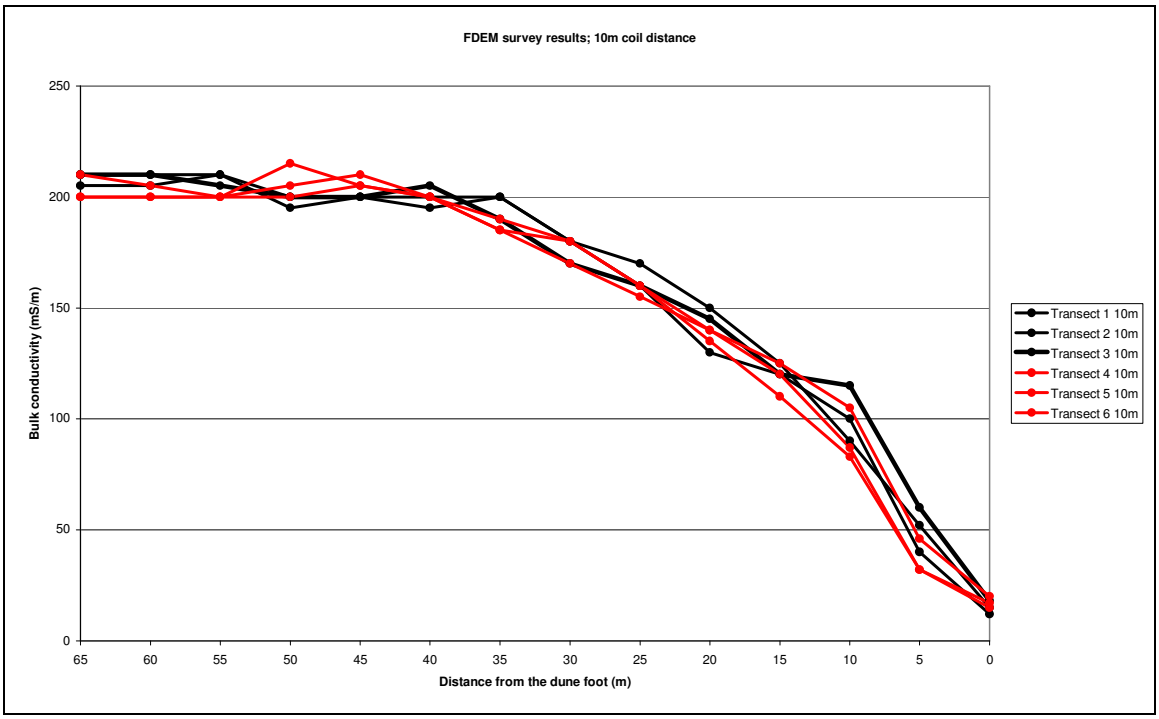
FDEM survey results; 10m coil distance
Bulk conductivity (mS/m)
250
200
150
100
50
0
65
60
55
50
45
40
35
30
25
20
15
10
5
0
Distance from the dune foot (m)
Transect 1 10m
Transect 2 10m
Transect 3 10m
Transect 4 10m
Transect 5 10m
Transect 6 10m

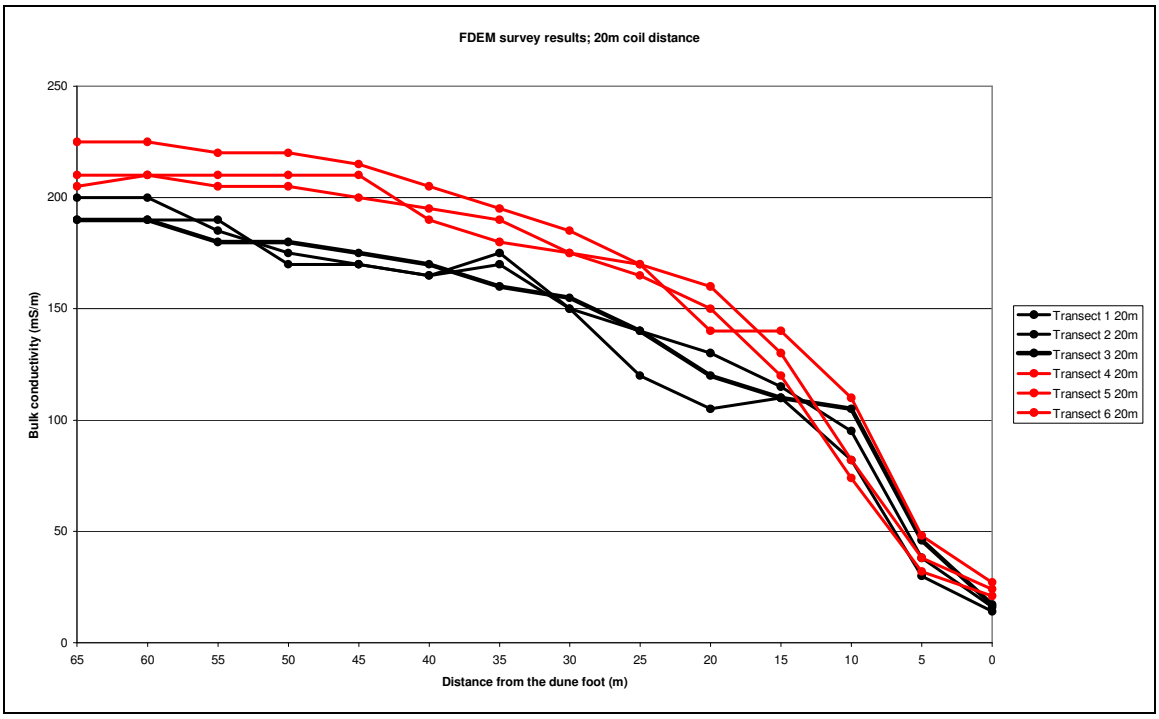
FDEM survey results; 20m coil distance
Bulk conductivity (mS/m)
250
200
150
100
50
0
65
60
55
50
45
40
35
30
25
20
15
10
5
0
Distance from the dune foot (m)
Transect 1 20m
Transect 2 20m
Transect 3 20m
Transect 4 20m
Transect 5 20m
Transect 6 20m

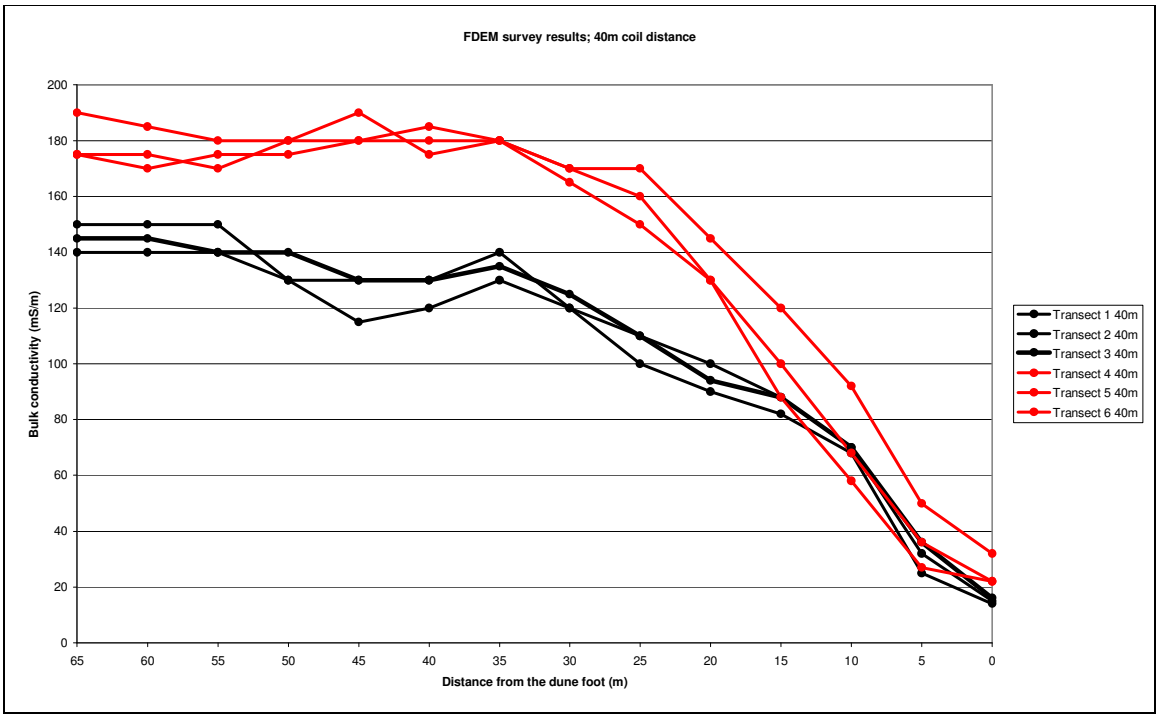
FDEM survey results; 40m coil distance
Bulk conductivity (mS/m)
200
180
160
140
120
100
80
60
40
20
0
65
60
55
50
45
40
35
30
25
20
15
10
5
0
Distance from the dune foot (m)
Transect 1 40m
Transect 2 40m
Transect 3 40m
Transect 4 40m
Transect 5 40m
Transect 6 40m